NASA TECHNICAL MEMORANDUM

NASA TM X-3555

NASA TM X-3555

EARLY PERFORMANCE OF THE 12-GHz, 200-WATT TRANSMITTER EXPERIMENT PACKAGE IN THE COMMUNICATIONS TECHNOLOGY SATELLITE

Lewis Research Center
Cleveland, Ohio 44135

NATIONAL AERONAUTICS AND SPACE ADMINISTRATION • WASHINGTON, D. C. • OCTOBER 1977

1. Report No.	2. Government Accession No.	3. Recipient's Catalog No.
NASA TM X-3555		

4. Title and Subtitle	5. Report Date
EARLY PERFORMANCE OF THE 12-GHz, 200-WATT TRANSMITTER EXPERIMENT PACKAGE IN THE COMMUNICATIONS TECHNOLOGY SATELLITE	October 1977
	6. Performing Organization Code
7. Author(s)	8. Performing Organization Report No. E-9104
	10. Work Unit No. 610-22
9. Performing Organization Name and Address National Aeronautics and Space Administration Lewis Research Center Cleveland, Ohio 44135	11. Contract or Grant No.
	13. Type of Report and Period Covered Technical Memorandum
12. Sponsoring Agency Name and Address National Aeronautics and Space Administration Washington, D. C. 20546	14. Sponsoring Agency Code

15. Supplementary Notes

16. Abstract

Measured performance characteristics of the transmitter experiment package (TEP) aboard the Communications Technology Satellite for the first 90 operating days in orbit are presented in this report. The TEP consists of a nominal 200-watt output stage tube (OST), a supporting power processing system (PPS), and a variable-conductance heat pipe system (VCHPS). The OST, a traveling-wave tube augmented with a 10-stage depressed collector, has an overall saturated average efficiency of 51.5 percent and an average saturated radiofrequency (rf) output power at center-band frequency of 240 watts. The PPS operated with a measured efficiency of 86.5 percent to 88.5 percent. The VCHPS, using three pipes to conduct heat from the PPS and the body of the OST to a 52-centimeter by 124-centimeter (20.5-in. by 48.75-in.) radiator fin, maintained the PPS baseplate temperature below 50° C for all operating conditions. The TEP performance characteristics presented include frequency response, rf output power, efficiency, and distortions. Communications characteristics were evaluated by using both video and audio modulated signals.

17. Key Words (Suggested by Author(s))	18. Distribution Statement
Communications Technology Satellite Traveling wave tube	Unclassified - unlimited STAR Category 17

19. Security Classif. (of this report)	20. Security Classif. (of this page)	21. No. of Pages	22. Price*
Unclassified	Unclassified	65	A04

* For sale by the National Technical Information Service, Springfield, Virginia 22161

FOREWORD

This report on the early (first 90 days of operation) performance of the transmitter experiment package (TEP) aboard the Communications Technology Satellite is presented in several discrete sections. While some minor overlapping and repetition among the sections is inevitable, this material organization provides maximum clarity. In addition to summary and introductory statements, the equipment and the general experimental procedures are described. Following these sections of the report are sections dealing, in turn, with TEP electrical, thermal, and communications performance. Each of the performance sections includes a description of the experimental procedures and test results specific to the evaluation performed. A separate section of the report then presents general conclusions and observations from all the performance tests included in the study.

The TEP performance studies and the preparation of this report were directed by Robert E. Alexovich, principal investigator in the super-high-frequency technology experiment. Many Lewis Research Center personnel contributed to the investigation, making complete individual recognition difficult. However, the authors of the report and their contributions are as follows:

ABSTRACT, SUMMARY, and INTRODUCTION - Robert E. Alexovich

DESCRIPTION OF EQUIPMENT and GENERAL EXPERIMENTAL PROCEDURES - Godfrey Anzic

INITIAL TEP TEST RESULTS:

Direct-Current and Radiofrequency Performance - Jerry Smetana and Clifford E. Siegert

Thermal Performance and Effects - Arthur N. Curren and Louis Gedeon

Communications Performance - Godfrey Anzic and Michael D. Richardson

Performance evaluation of future TEP operation will be published in subsequent reports.

CONTENTS

EARLY PERFORMANCE OF THE 12-GHz, 200-WATT TRANSMITTER EXPERIMENT PACKAGE IN THE COMMUNICATIONS TECHNOLOGY SATELLITE

Lewis Research Center

SUMMARY

The performance characteristics of the transmitter experiment package (TEP) aboard the Communications Technology Satellite (CTS) measured during its first 90 operating days in orbit are presented in this report. The TEP consists of a nominal 200-watt output stage tube (OST), a supporting power processing system (PPS), and a variable-conductance heat pipe system (VCHPS). The OST, a traveling-wave tube augmented with a 10-stage depressed collector, has an overall saturated average efficiency of 51.5 percent and an average saturated radiofrequency (rf) output power at center-band frequency of 240 watts. The PPS operated with a measured efficiency of 86.5 percent to 88.5 percent. The VCHPS, using three pipes to conduct heat from the PPS and the body of the OST to a 52-centimeter by 124-centimeter (20.5-in. by 48.75-in.) radiator fin, maintained the PPS baseplate temperature below 50° C for all operating conditions. The TEP performance characteristics presented include frequency response, rf output power, efficiency, and distortions. Communications characteristics were evaluated by using both video and audio modulated signals. The results are as follows:

1. Operation of a high-voltage (11.2 kV), high-power (570 W) electrical system has been demonstrated.

2. The TEP can support all CTS video and audio applications and provide high-quality communications.

3. An OST operating efficiency greater than 50 percent and a saturated rf output power greater than 200 watts were achieved.

4. There were no observable degradations in TEP performance due to launch, pre-injection, and operating environments or due to 90 days of in-orbit operation.

INTRODUCTION

Prior to the Communications Technology Satellite (CTS) program, NASA conducted extensive research with communications satellites. These spacecraft were placed in

low-intermediate and synchronous orbits and included passive reflectors, such as the 33-meter-diameter (108.3-ft-diam) Echo balloon; active repeaters, such as Relay and Syncom; and a series of Applications Technology Satellites (ATS), which investigated a broad range of communications technology and techniques. With each of the spacecraft, advances were made that permitted expanded use of the radiofrequency (rf) spectrum for satellite communications. Spacecraft effective radiated powers were increased by employing higher gain antennas and higher output rf amplifiers, or a combination of both.

The key to increased rf power for communications satellite applications is the development of high-power microwave amplifiers with high efficiency. As rf power output increases, high efficiency becomes more important. For high-power satellites, the efficiency of the transmitter, because of its large power consumption, directly determines the size of the solar array and the thermal radiator and the weight of the power processing system for the transmitter output amplifier.

The CTS program is a joint program of the United States and Canadian Governments. The CTS spacecraft was launched on a Thor-Delta 2914 launch vehicle on January 17, 1976, at 2327:54 Greenwich mean time (GMT) from the NASA Kennedy Space Center, Florida. It was injected into a geosynchronous orbit 35 887 kilometers (22 300 miles) above the equator and is stationed at 116° W longitude.

A salient characteristic of the CTS spacecraft that distinguishes it from prior communications satellites is its rf output transmitter power. It has simultaneous transmitter outputs of 20 and 200 watts. It uses two 85-megahertz bands centered at 14.052 and 14.247 gigahertz for uplink transmissions. These signals are translated to two 85-megahertz bands centered at 11.885 and 12.080 gigahertz and retransmitted to earth with rf output powers of 20 and 200 watts, respectively. Its rf output power of 200 watts is an order of magnitude greater than that of earlier communications satellites. This high rf output power is developed in the 85-megahertz frequency band at 12.080 gigahertz by the transmitter experiment package (TEP).

The TEP consists of a nominal 200-watt output stage tube (OST), a supporting power processing system (PPS), and a variable-conductance heat pipe system (VCHPS). The OST is a coupled-cavity, traveling-wave tube augmented with a multistage depressed collector. The PPS supports the operation of the OST by providing control for remote-command operation as well as protection and regulated operating voltages. The VCHPS is used to remove heat from the body of the OST and from the PPS.

Unique design approaches were used in achieving high efficiency - specifically, velocity tapering of the output coupled-cavity, slow-wave structure to achieve an interaction efficiency of 26 percent; a nine-active-stage (plus one at ground potential) multistage depressed collector (MDC) with beam refocusing to achieve a collector efficiency of 82 percent; and samarium cobalt magnets for output section focusing. In flight, these design approaches produced an OST average overall efficiency of 51.5 percent and an average saturated rf output power of 240 watts at center-band frequency. A two-stage

regulator composed of a switching chopper preregulator and a paralleled inverter for voltage scaling led to a dc-dc PPS efficiency of 86.5 percent to 88.5 percent. Stringent requirements were met for low output ripple, high regulation, and low stored energy.

The design approach selected for thermal control of the TEP was to use direct radiation from the MDC enclosure, which operated with a maximum in-orbit temperature of 180° C. A VCHPS composed of three pipes and a 52-centimeter by 127-centimeter fin radiator maintained OST body temperatures between 35° C and 60° C. This was accomplished for in-orbit operating conditions that resulted in heat rejection rates of 20 watts to 180 watts.

This report presents test results obtained from in-orbit tests conducted to evaluate the TEP. The period covered by this report consists of the first 90 days of TEP operation. This includes the period from the first start, which occurred February 8, 1976, to March 3, 1976, and the period from April 24 to June 13, 1976. Communications operations were discontinued during the eclipse period from March 4 to April 23, 1976, because of failure in the spacecraft power subsystem. Operations were resumed after that period. The results represent 90 TEP operating days (out of 154 days in orbit) with a total of 1233 hours of TEP operation in orbit. The TEP was also operated for 1800 hours in prelaunch testing.

In-orbit operating test results are presented for the OST, PPS, and VCHPS. Thermal in-orbit performance is presented for the OST, MDC, and VCHPS. In orbit, the OST and PPS have demonstrated operating efficiencies of 51.5 and 88.5 percent, respectively. Successful remote operation and self-protection of the high-power (570 W) PPS with output voltages of 11.2 kilovolts are described.

Communications test results for the high-power, high-efficiency TEP are presented. In-orbit saturated power output, frequency, and power transfer characteristics were unchanged from ground test results. Results obtained by using the TEP for single- and dual-channel frequency-modulated (FM) video transmissions demonstrate the TEP's capability to support the CTS communications applications with low-cost ground terminals.

The losses attendant on the large power consumption of the TEP necessitated special test techniques to accommodate widely varying heat rejection rates from both the OST body and the directly radiating MDC enclosure. Because the operating thermal environment is influenced greatly by its operating point, it was necessary to operate the TEP at constant rf power levels to achieve thermal equilibrium. This was done to establish repeatable test conditions. The thermal performance and effects are discussed in detail in this report.

DESCRIPTION OF EQUIPMENT

CTS TRANSPONDER: TRANSMITTER EXPERIMENT PACKAGE

The CTS super-high-frequency (SHF) transponder system provides two wide-band microwave downlink channels in the 12-gigahertz frequency band. The rf amplifiers used in both channels (20 and 200 W) are traveling-wave tubes (TWT). The higher power channel uses an advanced technology TWT with a multistage depressed collector (MDC), which contributes to the tube's high-efficiency operation.

The CTS SHF transponder consists of the following major elements:

(1) Two redundant receivers

(2) Two redundant low-power driver amplifiers

(3) Two high-gain receiving and transmitting antennas

(4) A switching and filtering system

(5) A high-power and high-efficiency microwave amplifier

(6) A power conditioning system

(7) An SHF beacon system

A block diagram of the major components of the SHF transponder is shown in figure 1. The frequency plan is presented in figure 2. The SHF transponder can simultaneously process signals in either of its two 85-megahertz-wide bands. A signal transmitted to the spacecraft in uplink band 2 (RB2) (see fig. 2) will be retransmitted to Earth in downlink band 2 (TB2) through the 20-watt TWT. A signal transmitted to the spacecraft in RB1 will be retransmitted to Earth in TB1 through the 200-watt high-efficiency TWT.

A major subassembly of the CTS spacecraft SHF transponder is the transmitter experiment package. This subassembly consists of the following major components:

(1) A power processing system

(2) An output stage tube consisting of the 200-watt traveling-wave tube and the multistage depressed collector

(3) A variable-conductance heat pipe system consisting of the radiator, reservoirs, and heat pipes

Power Processing System

Two spacecraft power sources supply direct-current (dc) power to the power processing system. These sources are the experiments bus, with a nominal voltage of 76 volts dc, and the housekeeping bus, with a nominal voltage of 27.5 volts dc. The PPS converts the spacecraft voltages to voltages ($\leq$11 200 V) needed for the operation of the high-power, traveling-wave tube. The PPS system physical dimensions and its

performance characteristics are shown in figure 3 and table I, respectively.

Two voltage protection circuits are also incorporated into the PPS in the event of an input over- or undervoltage malfunction. Additional circuits cause protective shutdowns because of excess OST body current or internal pressure. In addition, a number of voltage, current, and temperature measurements are interfaced through the PPS to the main spacecraft telemetry system. All telemetry data are encoded by one of two encoders. The data allocation is such that not all the TEP measured parameters are available unless the correct encoder is operating. The TEP telemetry measurement summary is presented in table II. The spacecraft command system is designed to accept 225 commands. The TEP responds to 20 commands whose sole function is to control the operation of the power, monitor, and protection circuits in the TEP. A list of TEP commands is presented in table III.

Output Stage Tube

The OST is a coupled-cavity, linear-beam, traveling-wave-tube amplifier (ref. 1). Highly efficient amplifier operation is realized through two major design features: a velocity taper in the slow-wave structure, and an MDC. The velocity taper synchronizes the bunched electron beam with the rf wave moving along the tube body to provide a high level of tube interaction efficiency (26 percent). The 10-plate depressed collector (nine active plates plus one at ground potential) sorts out and reduces the velocities of the spent-beam electrons so that the electrons are collected at near zero velocity, with low kinetic energy. This unique collector (ref. 2) produces efficient conversion of the spent beam kinetic energy to potential energy and lessens the amount of dc power required to operate the transmitter.

The OST performance specifications and physical details are presented in table IV and figures 4 and 5, respectively.

Variable-Conductance Heat Pipe System

The VCHPS supplements the OST baseplate thermal rejection capability by providing an additional 200 watts of heat transport from the baseplate when needed. Adequate heat rejection can be obtained in case one of the three heat pipes fails. The VCHPS mated to the TEP is shown in figure 6.

Transmitter Experiment Package Position in CTS Spacecraft

Views ot the CTS spacecraft are shown in figures 7 and 8. Relative positions and locations of the TEP and VCHPS can be seen, along with major spacecraft assemblies.

SUPER-HIGH-FREQUENCY GROUND STATION

The NASA Lewis Research Center SHF ground-station facility provides the main support for the TEP SHF technology experiment. The main operating requirements of the facility are

(1) To provide a high-power (85-dBW effective isotropic radiated power (EIRP)) wide-band, FM uplink signal to the spacecraft at 14 gigahertz (video and audio)

(2) To provide a low-noise, downlink receiving capability at 12 gigahertz (video and audio)

(3) To provide the capability of displaying video, audio, and telemetry data for real-time evaluation of electrical and communications parameters of the CTS transponder and TEP

The basic ground-station facility is shown schematically in figures 9 and 10. The facility characteristics are presented in table V.

The Lewis ground-station facility consists of three operational elements: the transmitter, the receiver, and the antenna.

Receivers, Modulators, and Transmitter

The high-power uplink transmitter consists of two identical low-power modulators, two low-power drivers, a two-channel combiner, and a high-power transmitter. Baseband video and audio signals applied to low-power modulators produce 14-gigahertz FM signals at their outputs. Either one or two FM channels may be processed through the channel combiner. The low-power, FM, video-audio channel is amplified in the low-power driver, the output of which is used to excite the high-power klystron. The high-power transmitter system employs two high-power klystrons (type VKU 7791) with a common power supply and common input-output circuitry. Only one klystron may be operated at a time. The characteristics of the klystrons are identical except for frequency. One is tuned for uplink band 1 (RB1); the other is tuned to uplink band 2 (RB2). Both klystrons are air cooled, and the entire transmitter system can be operated remotely (fig. 10).

A tunnel diode amplifier (TDA) is employed as a low-noise preamplifier for the dual-channel receivers operating at the downlink frequency of 12 gigahertz. The uplink-downlink system has the capability to generate and demodulate video carriers with a frequency deviation of 10 to 30 megahertz peak to peak with or without pre- or deemphasis.

Super-High-Frequency Antenna

The ground terminal antenna facility used to communicate with the CTS spacecraft consists of a 5-meter (16-ft) diameter parabolic reflector with a Cassegrain feed (fig. 11). The reflector, feed assembly, and pedestal (elevation over azimuth) mounting structure are mounted on the roof of a building at the Lewis Research Center. The associated tracking, controlling, and monitoring equipment is located in the EEC, which is in another building at Lewis. A step-track system, which is locked to a 11.7-gigahertz spacecraft beacon, can continuously update the antenna-pointing toward the spacecraft with an accuracy of ±0.05 degree.

Experiment Evaluation Center

The SHF experiment is conducted and evaluated from the EEC. The EEC serves as the main facility for displaying, switching, controlling, and evaluating video, audio, and telemetry data. Both the uplink transmitter and the 5-meter (16-ft) dish antenna can be controlled from this location. All audio and video signals (generated in a communications laboratory) are routed through the EEC to modulators. All signals received from the spacecraft are similarly routed through the EEC to various display and recording equipment, which includes video tape recorders.

Sample Link Calculations

Tables VI and VII show typical uplink and downlink power budgets for the wide-band video signal being processed through the spacecraft transponder's 200-watt channel. Although the spacecraft employs two redundant receivers, the power budgets presented use the primary receiver's characteristic noise temperature of 1315 K (parametric amplifier). The secondary spacecraft receiver contains a TDA with a noise temperature of 2315 K. Received video quality is slightly reduced when the secondary receiver is used. (The parametric amplifier was used for all tests conducted to date.) The uplink and downlink power budgets are presented for two transponder saturated gain conditions. The transponder maximum gain condition of 125 decibels may be reduced to 120 decibels by commanding in a switchable attenuator (fig. 1). In addition to the 5-decibel transponder gain reduction, 10- and 15-decibel gain reductions are possible but have not been used.

The sample uplink power calculation summarized in table VI presents the power requirement to saturate the OST on the spacecraft. The power budgets shown contain a

general power margin (3.0 dB each for uplink and downlink) and rainfall attenuation margin (2.23 dB on uplink and 1.52 dB on downlink). In most cases, only a fraction of this total margin is used. As an example, the uplink power required to saturate the OST was typically 2 decibels higher than the minimum predicted value, which excludes all margin, rain attenuation, and antenna-pointing errors (table VIII). Calculated values of both uplink power requirements and video signal-to-noise ratios are within acceptable limits of comparison to actual measured values if allowances are made for measurement inaccuracies and uplink-downlink signal attenuation due to weather conditions. Weather conditions for the test periods of this report are shown in figure 12. These data were obtained from the National Weather Service station located at Cleveland Hopkins Airport. This station is about 3 kilometers (2 miles) east of the Lewis ground station. Figure 13 shows the CTS beacon signal attenuation experienced at the ground station during a test period. Included in the same figure is the rain rate recorded at the Cleveland weather station. Attenuations as large as 17 decibels were experienced during periods of heavy rainfall.

GENERAL EXPERIMENTAL PROCEDURES

Operation of the TEP was begun at about 0912 EST on February 8, 1976, shortly after the CTS spacecraft was placed in geosynchronous orbit at 116° W longitude. A series of tests was immediately begun to determine the in-orbit communications, electrical, and thermal performance of the TEP. Table IX presents a list of the tests and the schedule of their execution through June 14. All the TEP tests were conducted at the Lewis Research Center SHF ground-station facility with its computer data reduction capability. For these tests, the spacecraft antennas were commanded to the ground-station coordinates for optimum operation of both uplink and downlink systems. In a typical test, an uplink signal format was transmitted to the spacecraft, and the signal returned from the spacecraft was evaluated by the ground station. The results and implications of these tests are treated in detail in the remainder of this report. Each of the tests in table IX was performed according to its own specific procedure, which will be detailed along with the test results. The results of some tests were sensitive to spacecraft component selection. For example, TEP video performance varied with the amount of attenuation in switchable attenuator 2 (fig. 1). In those cases, various spacecraft components were selected to identify the optimum practical performance configuration.

Because of large power consumption, the TEP operation has a great effect on its thermal environment. The experimental evaluation was conducted with the TEP at thermal equilibrium. Thermal test results were observed to be sensitive not only to TEP

operating conditions but also to the orbital position of the spacecraft relative to the Earth and the Sun and the time of the year (i. e., the Sun declination angle).

For those tests that displayed a sensitivity to changing TEP temperatures, an acceptable level of thermal equilibrium was achieved.

INITIAL TRANSMITTER EXPERIMENT PACKAGE TEST RESULTS

ELECTRICAL PERFORMANCE

The data used to evaluate the electrical performance of the TEP were taken after the TEP had been operated for 2 hours to achieve thermal stability. The operating points were

(1) Radiofrequency output power: saturated, 100 watts, and zero rf

(2) Frequency: lower band edge, 12.038 gigahertz; center band, 12.080 gigahertz; and upper band edge, 12.123 gigahertz

(3) Spacecraft position: 0^{o}, 90^{o}, 180^{o}, and 270^{o}

The spacecraft position, which is described in detail in the section OUTPUT STAGE TUBE AND HEAT PIPE SYSTEM THERMAL PERFORMANCE, is the location of the spacecraft in the Sun-Earth coordinate system.

Efficiency

Two basic components of the TEP are the PPS and the 200-watt TWT, often called the OST. The efficiencies of these components are described separately.

PPS efficiency. - The efficiency of the PPS was examined for the first 90 days of operation. It was calculated at 24 different times. The power that was drawn from the experiments array varied from 443.82 watts to 561.42 watts. The experiments array voltage varied from 81.71 volts to 83.49 volts. This voltage variation is a function of the amount of power drawn from the array and the sunlight incident on the solar array. The PPS baseplate temperature varied from 36.6^{o} C to 48.8^{o} C. This temperature variation is a function of the amount of power being delivered to the OST and also the sunlight incident on the south panel of the spacecraft. To calculate PPS efficiency, both the power drawn from the two solar arrays and the amount of power delivered to the OST had to be calculated. The input power to the PPS was taken as the sum of the power from the 27.5-volt array and the experiments array less 7 watts accountable to the PPS telemetry. The power delivered to the OST was obtained by summing the collector power, the anode power, the cathode heater power, and the power loss due to electron beam defocusing. The efficiency was then calculated from the ratio of power delivered

to the OST and power drawn from the solar arrays. As shown in table X, the PPS efficiency varied from 86.56 percent to 88.51 percent. This range of efficiency is in close agreement with the efficiencies calculated during ground testing of the PPS.

OST efficiency. - OST efficiency was computed by dividing the rf output power measured by the forward power monitor (FRWD) on the spacecraft by the total dc power delivered to the OST. Figure 14 shows the 200-watt TWT overall efficiency as a function of frequency. The largest and smallest value at each frequency were plotted during the first 9 days in orbit and for the following 81 days of operation. The values measured during the thermal vacuum testing before launch and those measured on the 82nd day of testing were also plotted. The line is the mean value of all the ground thermal vacuum test and flight data.

In figure 15, all the data for the center-band, saturated condition were plotted to show the variation of efficiency with time. There is little change in performance with time during the first 90 days of operation. The mean efficiencies of the data shown (51.78 and 51.48 percent) and the standard deviations (1.53 and 2.16 percent) were computed for the period before and after the eclipse. Although these values are higher than expected, they do confirm consistent operation. The high values are due to the calibration of the forward power monitor discussed in the next section.

Radiofrequency Power Output

Figure 16 is a plot of the 200-watt TWT output power during the first 90 days of operation. The power was measured by using a detector diode in the forward power monitor at the output port of the 200-watt TWT on the spacecraft. There appears to be no deterioration of the output signal. The mean output powers (23.84 and 23.82 dBW) and the standard deviations (0.08 and 0.19 dB) before and after the eclipse period confirm consistent operation. The mean output is about 0.25 decibel higher than expected from thermal vacuum test data. This is attributed to uncertainty in the forward power monitor sensor calibration. The sensor was calibrated during the thermal vacuum test at five equally spaced frequencies from 12.038 gigahertz to 12.123 gigahertz and over an output coupler temperature range of -5° C to 60° C. The measured values of this temperature in orbit were as high as 84.5° C; therefore, extrapolation of the calibration became necessary.

Beam Focusing

Measuring the current (body current) from the OST body to the PPS common gives an indication of beam focusing. The body current measured at saturated output during the first 90 days of operation is plotted in figure 17. The mean body currents (6.30 and

6.46 mA) for the periods before and after the eclipse period show a small increase with time, but the difference is within the standard deviation. There are insufficient data to conclude that body current is increasing, especially in light of the consistency of the efficiency and output power data (section Efficiency).

The high and low values of these data at saturated output were plotted against frequency in figure 18 and compared with values obtained in the thermal vacuum test and the test on the 82nd day of operation. The OST prelaunch thermal vacuum test data are within the range of the variation of in-orbit data. Therefore, it may be concluded that there is agreement between prelaunch and in-orbit data and that the most probable variation of body current with frequency at saturated output power is the average of all data as shown. Figure 19, a plot of body current at 100-watt rf output power, shows the variation of body current with frequency. In figure 20, the high and low values of body current at nominal TEP output powers of 0, 100, 200, and 230 watts were plotted to show the mean value of body current as a function of output power. The value at zero rf represents the best beam focusing, where a minimum number of electrons impinge on the OST body as the beam passes through the coupled-cavity section. As the beam is modulated when rf drive is applied, there is a distortion of beam focusing, and more electrons impinge on the OST body.

Cathode Life

The OST beam current was monitored continuously to observe cathode performance. The beam current changed from 76.6 milliamperes to 76.2 milliamperes during the first 90 days of operation. This change represents one count of digital telemetry data from the CTS spacecraft. The current remained at the 76.6-milliampere level after the eclipse period and dropped to the lower value about 85 days after the first TEP turnon.

The change in beam current, about 0.5 percent, was less than the accuracy of the telemetry system (1.0 percent). It can be concluded that the cathode is operating normally and that there has been essentially no change in its performance.

High-Voltage Space Operation

High-voltage leakage. - The high-voltage leakage currents in the PPS and OST were determined by applying high voltages with the cathode heater in the off state. Measurements of high-voltage currents were made before initial operation of the TEP and again after 75 days of operation. No measurable leakage currents were observed before initial operation of the TEP in space and after 75 days of operation. Therefore, it is con-

cluded that there has been no increase in high-voltage leakage currents in the PPS and OST due to launch, preinjection, or operating environments.

Outgassing. - The TEP was tested twice in vacuum as an integrated system before launch. During each of these tests, the first turnon of high voltages was monitored very closely to determine any anomalous operation that could be attributed to OST internal outgassing. The anomalous operation would be indicated by shutdowns due to internal arcing. During ground tests, the TEP was subjected to a minimum of 72 hours in vacuum before high voltages were turned on. There was no evidence of outgassing during the ground tests or during operation in space.

OST internal pressure measurements were monitored continuously. During the first 9-day test, the pressure varied from 0.7×10^{-7} torr to 1.0×10^{-7} torr. Over the first 90 days of spacecraft operation, the pressure range was 0.5×10^{-7} torr to 1.0×10^{-7} torr. These pressure ranges are normal and were experienced in ground testing.

OUTPUT STAGE TUBE AND HEAT PIPE SYSTEM THERMAL PERFORMANCE

The purpose of this portion of the investigation was to thermally characterize the 200-watt OST and the VCHPS in important operating modes for several spacecraft orbit positions. Specifically, the objectives of this continuing thermal investigation are

(1) To determine if critical component temperatures remain within prescribed limits

(2) With frequent reexamination of thermal characteristics, to identify possible long-term performance changes

(3) To identify thermal conditions that will typify periods of communications use

(4) To acquire thermal characteristics data that may be used to aid in possible spacecraft problem diagnosis

(5) To provide fundamental thermal performance data for application to future programs of a related nature

Instrumentation

The locations of the thermal instrumentation routinely monitored to perform this investigation are identified in figures 21 and 22. The instruments (all thermistors except where noted) are identified in the figures and in the text by their computer-code descriptive symbols. In addition to the thermal instrumentation, the characterizations developed during this study required the use of quantities measured by other methods that are described elsewhere in this report. These other quantities include OST body current, OST input dc power, and OST output rf power and frequency.

Output stage tube. - As shown in figure 21, four thermistors are used to measure the temperatures on the OST. One of these, MDC1, is located on the cylindrical cover of the MDC section of the tube. This MDC cover is coated with a paint having a high thermal emittance and is cooled by direct radiation to space. Another thermistor, MDC2, is located on the MDC high-voltage feedthrough flange just inboard of the MDC cover thermal choke (the bellows-like configuration in fig. 21). The remaining two sensors, BODY and CPLR, are attached to the heavy copper "isothermalizer" bar on the tube body at the output waveguide transformer position and at the output power diode sensor position on the output waveguide coupler, respectively.

Variable-conductance heat pipe system. - The VCHPS, shown schematically in figure 22, consists of three variable-conductance heat pipes that transfer heat from an evaporator saddle located under the OST baseplate to an isolated radiator panel just adjacent and coplanar to the south spacecraft radiator panel. Six temperature sensors are located on the VCHPS, as indicated in figure 22. One thermistor is located on the adiabatic section of each heat pipe. These instruments, HP1T, HP2T, and HP3T, are attached to heat pipes designated 1 (shortest), 2, and 3 (longest), respectively. Thermistor HP4T is attached to heat pipe 1 a short distance (4 cm (1.57 in.)) further along the pipe from HP1T. Two additional instruments, HP5T and HP6T, both platinum resistance thermometers, are positioned further along on heat pipe 1. Sensor HP5T is attached near (4 cm (1.57 in.)) the end of the inert-gas reservoir, and HP6T is attached directly to that reservoir.

A thermistor, BPLT, located nearby on the baseplate of the power processor portion of the TEP is useful under some conditions as an additional indicator of VCHPS performance.

Test Procedures

The thermal testing program has consisted of three related efforts. These are OST thermal equilibrium tests, regular VCHPS checks at key operating periods, and continuous monitoring of several important OST and VCHPS temperatures.

OST thermal test conditions. - The OST thermal tests are all performed at the thermal equilibrium condition, since that condition provides a relatively repeatable comparison point. Further, since the test periods generally begin with the OST operating at other than the selected test condition, the time required for the OST to achieve thermal equilibrium is simultaneously determined during each test. A good knowledge of this thermal time characteristic is important for preeclipse operation planning to ensure that key OST temperatures remain in a safe range during eclipse periods.

Most of the thermal tests reported in this study were performed at the OST operating conditions expected to be most common. Specifically, these are saturated rf output power at center-band frequency (12.080 GHz), 100-watt rf output (nominally, saturation minus 3 dB) at center-band frequency, and zero rf output (the dc beam condition). In addition, saturated and 100-watt rf output power tests were also performed at the upper-band-edge (12.123 GHz) and lower-band-edge (12.038 GHz) frequencies, which are intended to represent worst-case operating conditions. With a few exceptions, the tests were performed while an unmodulated carrier signal was being transmitted.

Spacecraft orbital positions. - To allow comparison, most of the OST thermal equilibrium tests were conducted at one of four selected spacecraft orbital positions, separated by 90°. These orbital positions are shown schematically in figure 23. The first position, designated as 0°, is the spacecraft midnight position. As first indicated in prelaunch thermal vacuum tests at Lewis, approximately 2 hours is required for the OST to achieve thermal equilibrium after a condition change. Consequently, a thermal test typically is begun about 1 hour before the spacecraft is in the desired orbital position and is continued about 1 hour beyond.

Each of the spacecraft orbital positions feature distinctly different solar illumination and solar array orientation conditions. These conditions directly affect the thermal environment of the spacecraft south panel radiator surface, the VCHPS radiator surface, and the OST MDC enclosure, which is also a radiator surface. The thermal conditions of these surfaces, in turn, directly affect the OST baseplate temperature and consequently the OST performance. Therefore, one of the objectives of this test series is to thermally characterize the OST and VCHPS relative to operating conditions for each of the selected orbital positions. This information may be required for the interpretation of any effects that are regarded as unusual during later user and technology experiments.

Sun angle effects. - Because the Sun incidence angle relative to the spacecraft orbit plane progressively changes throughout the year, the spacecraft experiences day-by-day changes in thermal environment independent of the orbital position and the OST operating conditions. The Sun angle relative to the Earth equatorial plane (taken here to closely approximate the spacecraft orbital plane) at the spacecraft noon (180°) orbital position is shown in figure 24. Therefore, in addition to the requirement of determining the thermal characteristics of the OST and VCHPS for the various operating conditions and spacecraft orbital positions, the effects of the variation of the solar flux incidence angle must also be determined for complete characterization.

VCHPS condition monitoring. - In addition to the VCHPS temperature data taken during the OST thermal equilibrium test periods, the several temperatures that define the performance of this thermal control system are examined frequently. This is particularly necessary when the OST experiences changes in operating conditions that rapidly change VCHPS temperatures. Such situations, for example, occur at OST turnon

periods, particularly after a relatively long period when the OST has not been operated. The objective of this monitoring is to regularly evaluate the starting and operating conditions of the VCHPS and to document the anticipated long-term degradation of the optical properties of the radiator.

Several VCHPS and OST temperatures are also monitored continuously on strip-chart recorders and are regularly examined. This monitoring is done to ensure that unanticipated temperature excursions that might occur during nonspecific thermal test periods can be quickly detected and evaluated.

Output-Stage-Tube Thermal Test Results

As has been indicated, the OST tests were all performed at the thermal equilibrium condition. That condition is defined as that time when all monitored OST temperatures remain stable within 1 degree C for at least 5 minutes. For most of the tests performed, the monitored VCHPS temperatures met this criterion as well.

A typical OST thermal transient period is depicted graphically in figure 25. Just before the establishment of the desired conditions for this test, the OST had been in the "standby" mode, with only the cathode heater at 50 percent power (~2 W) for some time. As a result, the OST and VCHPS temperatures were all at a relatively depressed level. The test conditions (saturated rf output power at lower-band-edge frequency) were established at the turnon point indicated in figure 25, with the resulting time-temperature profiles shown. As indicated in this figure (and typically), approximately 2 hours was required for the OST to achieve thermal equilibrium after a condition change. In general, the OST thermal data presented in this report are the first data points taken after the requirement of thermal equilibrium has been met.

Initial OST testing period results. - Because of the day-by-day variation of the Sun incidence angle with the spacecraft orbital plane, it is difficult to rigorously evaluate by comparison the results of thermal tests run at identical OST operating conditions even a few days apart. Nevertheless, figure 24 shows that a significant number of thermal tests were conducted in a relatively short time during which the Sun angle changed by only about 8°. During this time, from February 9 to March 3, the Sun was below the Earth equatorial plane and illuminated the spacecraft south panel and the VCHPS radiator panel. This initial series of tests, then, represents a convenient and useful, although nonrigorous, data comparison, which is examined in this section of this report.

Figure 26 shows the equilibrium profiles for the MDC cover temperature, MDC1, and heat pipe 1 temperature, HP1T, for several OST operating conditions at the various spacecraft orbital positions for the initial OST testing period. When heat pipe 1 is active (HP1T $\geq 25^{\circ}$ C, approx.), HP1T approximates OST baseplate temperature.

Figure 26 shows the measured MDC1 temperatures to be lowest at all orbital positions for the saturated rf output power at center-band frequency conditions. This temperature characteristic at the point of measurement was also observed during prelaunch thermal vacuum testing of the OST. The MDC cover temperature variation for essentially constant operating conditions as a function of orbital position is attributable to the differences in solar illumination on the cover. Figure 23 shows that the MDC cover receives very little direct solar illumination at the 0^{o} orbital position but that maximum illumination is experienced at the 180^{o} position. Consequently, the maximum and minimum MDC cover temperatures occur at the 180^{o} and 0^{o} orbital positions, respectively, for this initial testing period.

The HP1T temperature profiles shown in figure 26 are fairly level except for a modest depression at spacecraft orbital positions other than 0^{o}. At 0^{o} the inboard heat pipe radiator surface receives a greater amount of reflected solar illumination than at other orbital positions. Data for test conditions other than the saturated-rf-output-power, center-band-frequency condition are characterized by somewhat lower HP1T temperatures because of lower rf output power and OST body-current levels.

Equilibrium profiles for the OST body temperature, BODY, and the output waveguide coupler temperature, CPLR, for the operating conditions and spacecraft orbital positions (same test points) of figure 26 are shown in figure 27. For a given orbital position, both temperatures increase with increasing rf output power (with accompanying increasing rf attenuation losses) and OST body current. The BODY and CPLR temperatures are generally slightly lower at orbital positions other than 0^{o} because of the influence of the HP1T temperature characteristics.

Second OST testing period results. - When the Sun angle relative to the spacecraft orbital plane became zero on March 20 and then became increasingly positive (fig. 24), direct solar illumination of the spacecraft south panel radiator and VCHPS south radiator surface was reduced to and remained at zero throughout the remainder of the reporting period described in this study. Therefore, aside from the day-by-day Sun angle variation effects on the MDC cover temperature, the other OST and VCHPS temperatures were relatively unaffected by the influence of solar illumination of the VCHPS south radiator surface during this posteclipse testing period. Consequently, this period presents an opportunity for test data comparison similar to the initial OST testing period.

Figure 28 shows the MCD1 and HP1T temperatures as a function of OST operating conditions and spacecraft orbital position. As expected, the MDC1 temperatures were lowest for each orbital position for saturated rf output at centerband frequency. In general, the MDC1 and HP1T temperature levels were lower for each orbital position than those observed in the preeclipse tests of figure 26. The apogee motor nozzle and adjacent struts shadow the MDC cover at the higher Sun angles during the posteclipse period. This shadowing accounts for the lower posteclipse MDC temperatures relative to the preeclipse temperatures.

The HP1T temperature profiles of figure 28 are also generally lower than their preeclipse counterparts because of the lack of direct solar illumination of the south surfaces of the spacecraft and the VCHPS radiator. Here, the 0^{o} orbital position temperatures are slightly higher than the others because of the shadowing of the inboard VCHPS radiator surface by the antennas at the 90^{o} and 270^{o} orbital positions and by the body of the spacecraft itself at the 180^{o} position. Heat pipe 1 is apparently not active in the posteclipse tests at the low OST body heat-rejection-rate level of the dc beam tests. The HP1T temperatures for these tests are, therefore, not indicative of the OST baseplate temperature.

Figure 29 presents the equilibrium profiles for the OST body temperature, BODY, and the output waveguide coupler temperature, CPLR, for the same test points of figure 28. For both of these plots, at any given spacecraft orbital position, the temperature increases with increased rf output power and attendant increased rf attenuation losses along with an increase in OST body current. Both profiles are generally lower in temperature level than their preeclipse counterpart test points because of the posteclipse lack of direct solar illumination on the south surfaces of the spacecraft and the VCHPS radiator. Also evident from these profiles are the generally lower temperatures at orbital positions other than 0^{o} due to inboard (north facing) shadowing of the VCHPS radiator surface by the antennas and spacecraft body. Maximum shadowing of the north-facing VCHPS radiator surface occurs at the 180^{o} orbital position, as evidenced by the diagram of figure 23 and the temperatures of figure 29.

Tests results summary. - In addition to the effects on OST and VCHPS thermal performance of general OST operating conditions, spacecraft orbital position, and Sun angle with the orbital plane, the effects of simple operational variations need to be considered. While the influence is assuredly relatively small, occasional (for example) minor brief deviations in uplink (to spacecraft) transmitted power level and/or frequency can and do induce small temperature perturbations that are reflected in the test data. Further, changing atmospheric conditions and ground antenna-pointing cycles also cause similar brief changes in OST operation that influence the data. Based on the limited experimental information presented in the preceding sections, it is not reasonable to attempt to precisely predict OST and VCHPS temperatures for all operating conditions at all spacecraft orbital positions and all Sun angles. Nevertheless, based on the data taken, it is reasonable to present typical values or ranges of values that can be expected for the various conditions studied, assuming that OST performance characteristics remain relatively unchanged. These values appear in table XI. Significant excursions of parameter values away from those ranges shown in table XI may be viewed as possible indications of OST, PPS, or VCHPS performance changes.

As was indicated earlier, one of the objectives of this study is to identify possible long-term OST performance changes. To the time of this report, no measurable evi-

dence of change was observed. Within the anticipated limits of data reliability, the OST thermal performance and parameter repeatability for similar operating conditions has been excellent. The BODY and CPLR temperatures and OST body-current levels have been essentially constant relative to rf output power and frequency. Other general observations concerning OST thermal performance are

(1) Measured critical OST component temperatures remain well within the limits established for worst-case flight predictions in reference 3.

(2) As has been indicated, about 2 hours is required for the OST to achieve thermal equilibrium after a condition change.

(3) OST rf performance is normal throughout an OST thermal transient period.

Variable-Conductance Heat Pipe System Thermal Performance

As has been described, the VCHPS transfers heat from an evaporator saddle located beneath the OST baseplate to an isolated radiator panel adjacent and coplanar to the south-facing spacecraft radiator panel. The system is shown schematically in figure 22. The three heat pipes, designated 1 (shortest), 2, and 3 (longest) are dual-artery, stainless-steel pipes. Methanol is the medium fluid and a mixture of nitrogen (90 percent) and helium (10 percent) is the inert regulating gas. The system is designed so that as heat input to the evaporator saddle is increased from very low levels, heat pipe 1 becomes active first, followed by pipes 2 and 3 in that order. As the heat input is increased, the active length of the heat pipes and, consequently, the active area of the radiator to which the pipes are attached increase. With this system, the heat pipes are considered to become active, or turn on, when the temperatures indicated at the locations of HP1T, HP2T, and HP3T reach a level of about 25° C to 30° C. The active length of heat pipe 1 is intended to be indicated by the three other temperature sensors located further along its length - HP4T, HP5T, and HP6T.

VCHPS startup and shutdown characteristics. - The CTS OST was first put into full in-orbit operation on February 8. Figure 30 shows time profiles of the VCHPS HP1T, HP2T, HP3T, and HP4T temperatures, as well as the OST body temperature, BODY, for the ensuing several hours. Included also is a curve illustrating the TEP input power for that time. The rf output power of the OST is at saturation (~240 W) for peak values of the TEP power curve in the figure. The heat-pipe startup sequence is shown in the proper order, with pipe activation occurring at about 30° C at approximately 1020 EST and then gradually increasing as BODY temperature increases. With the VCHPS active to this extent, the BODY temperature could be maintained at 52° C with the PPS baseplate temperature, BPLT, at 36° C. Sensors HP5T and HP6T were not affected by the heat input at the evaporator. For the time shown in figure 30, HP5T

changed from -50° C to -73° C, and HP6T changed from -38° C to -53° C. Heat pipe 1 is not designed to fully activate as long as all three pipes are operational.

A VCHPS shutdown sequence, a number of which have been observed, is essentially the reverse of the startup sequence. The OST was put into operation for the second (posteclipse) testing period on April 20. The VCHPS startup sequence for that event is shown in figure 31. Comparing the TEP power input schedules of figures 30 and 31 reveals quite different starts, which result in significantly different VCHPS startup sequences. As with the first startup, the sequence of figure 31 shows the heat pipes turning on, in order, at about 30° C. Preceding the turnon point is a significantly abrupt drop in all heat-pipe temperatures followed by rapid recovery as TEP power is increased. This temperature drop is apparently due to cold methanol being drawn to the evaporator as pipe function begins, with subsequent cooling of the sensors as it passes. Similar temperature fluctuations have been observed in other VCHPS startup sequences, but in most of those, the temperature drops have been only about 2° C to 5° C. Apparently, the long time period over which the TEP was brought to full power in this start (~$4\frac{1}{2}$ hr) exaggerated the temperature perturbation. Normally, the TEP would be brought to full power in just a few minutes. It appears that the gas vapor front moves toward the condensor portion of the VCHPS more rapidly with a faster startup, thereby reducing the cooling effect at the sensor locations. In any event, this temperature peculiarity apparently does not interfere with VCHPS functioning.

VCHPS thermal performance summary. - To the time of this report, the VCHPS has functioned thermally as designed, turning on and off as required to maintain the temperatures of the components of the TEP (including the OST) within the limits prescribed in reference 2. The PPS baseplate temperature was maintained below 50° C for all operating conditions. Spacecraft limitations prevent sufficient onboard thermal instrumentation to permit in-orbit determination of whether the heat pipes are all completely functional, since gas front locations cannot be determined.

COMMUNICATIONS PERFORMANCE

Transponder Video and Audio Tests

Video and audio communications tests were performed to evaluate the TEP as an element of a space communications link. Both quantitative and qualitative data were taken in order to completely describe the TEP's performance. Equipment conforming to National Television Systems Committee (NTSC) specifications was used in all video tests. For video signal-to-noise measurements, a noise comparison technique was used. The technique is discussed in detail in reference 4. All video signal-to-noise

measurements given are unweighted. To arrive at a weighted, International Radio Consultative Committee (CCIR) signal-to-noise measurement, a noise weighting factor of 12.8 decibels must be added. Qualitative performance was evaluated by an expert observer using the rating scale shown in table XII. All video tests were performed under the following conditions:

(1) Video modulation index of 2 (18-MHz peak-to-peak deviation)

(2) Video pre- and deemphasis per CCIR recommendation 405-1 for 525-line system

(3) Signal-to-noise measurements made by using standard video test signals with no audio subcarriers present

Single-channel video tests. - Single-channel video tests in TB1 were performed in the lower, center, and upper bands. The results of these tests are summarized in table XIII. The measured video characteristics for the single-channel mode are very good. Subjective evaluations by expert observers have shown that a differential gain dG of 10 percent and a differential phase $d\varphi$ of 5° have a barely perceptible effect on the video picture. From table XII, worst-case dG (4 percent) and worst-case $d\varphi$ (4.5°) occurred at a number of operating points and reflect the total ground-station and transponder system. These worst-case values are well within the limits quoted for $d\varphi$ and dG for high-quality performance. The worst-case signal-to-noise ratio, 41 decibels, was at 12.101 gigahertz at saturation minus 3 decibels. A signal-to-noise ratio of 40 decibels or greater is considered excellent. The signal-to-noise ratios shown in table XIII increase as the TEP output power decreases beyond saturation. This is expected since the uplink carrier-to-noise ratio increases as uplink power increases.

Dual-channel video tests. - Quantitative and subjective tests were performed to determine the uplink carrier amplitudes and 200-watt TWT operating point that produces minimum video crosstalk between two video channels transmitted in the RB1/TB1 band. Figure 32 summarizes the results of the tests for a frequency separation of 50 megahertz (channel 1, 12.055 GHz; channel 2, 12.105 GHz). Normally, when operation is in the dual-channel mode, equal downlink carriers are preferred in order to obtain acceptable signal-to-noise ratios at receivers tuned to each of the channels. The channel 1 uplink carrier must be 3 decibels higher than the channel 2 uplink carrier in order to obtain equal downlink carriers. Figure 32 indicates that for this operating condition ($P_{ch1} = P_{ch2} - 3$ dB on the uplink), the crosstalk levels from channel 1 to channel 2 increase with increasing TEP input power. Subjective evaluations of test signals confirm this. At saturation plus 3 decibels the interference is barely perceptible but not annoying, and at saturation minus 3 decibels the interference is imperceptible. For this same configuration, the crosstalk level from channel 2 to channel 1 decreases with increasing TEP input power. Subjectively, the observed video crosstalk was imperceptible for coupling from channel 1 into channel 2.

The optimum conditions for dual-channel operation were

(1) Channel 1, 12.055 gigahertz

(2) Channel 2, 12.105 gigahertz

(3) $P_{ch1} = P_{ch2}$ - 3 dB uplink carrier

(4) TEP operated at saturation (70 W/channel at tube window)

(5) Signal-to-noise ratio, 46 decibels for both channels

These conditions are based on cochannel interference levels as well as downlink amplitudes.

The measured signal-to-noise ratio, $d\varphi$, and dG reflect ground-station receiver characteristics as well as transponder operation. The ground-station signal-to-noise ratio, $d\varphi$, and dG may be considered negligible since these parameters have been optimized to produce minimum signal distortion. Ground-station video system characteristics are

(1) Signal-to-noise ratio, 58 decibels

(2) Differential gain, 1.5 percent

(3) Differential phase, 0.7^{o}

The quantitative interference measurements reflect transponder operation as well as ground-station receiver characteristics. Since intermodulation in the transponder is one of the mechanisms that produces video interference, the frequency response of the receiver front-end filter system affects the interference levels measured. A receiving system with a sharper-slope filter skirt would yield less interference. A broader-slope filter skirt would yield higher interference levels.

Dual-channel audio tests. - A swept-frequency test of the audio channels associated with video in the lower and upper bands in TB1 was performed to determine the system frequency response. There was no degradation. The limiting factor in this test was the response of the modulator-demodulator pair used in the ground-station system. Since the measured response was within the modulator-demodulator specifications, no measurable degradation is attributable to the TEP.

Multichannel telephone test. - White-noise loading techniques were used to simulate a multichannel telephone traffic condition. Two telephone channel capacities were simulated: 60 and 960 channels. The test was performed using equipment conforming to CCIR recommendation 399-1, which deals with baseband loading levels and filter characteristics associated with the white-noise loading technique. The unit dBrnc (decibels above reference noise) is C-message weighted, which is in current use by the common carriers. The noise levels recorded in table XIV reflect the total SHF spacecraft communications link. The main contributor to the measured intermodulation noise is the spacecraft TEP/transponder TEP system, since the gound-station noise levels are at or below the threshold of the noise test set. Subjective tests have shown that noise levels of 31 dBrnc are rated excellent by 50 percent of observers. Table XIV summarizes the results. The multichannel telephone performance of the TEP/transponder system is excellent. Although operation at lower power levels (saturation minus 3 and 6 dB) yields higher noise levels, the performance (e.g., 38.3 dBrnc) is

rated very good by subjective tests. Table XIV shows an increase in noise power as the TEP output power is decreased. This result is to be expected since a decrease in TEP input power results in a lower carrier-to-noise ratio at the input. The measurement results for reduced input signal levels are determined predominantly by additive noise and are not due to intermodulation.

Frequency Response

Swept-frequency response was measured and compared with previously taken ground data. Any change in the response characteristic between in-orbit and ground tests would indicate a possible shift in the TWT operating characteristics. Swept-frequency response curves taken during thermal vacuum testing are compared with in-orbit results in figure 33. Based upon thermal vacuum data and the two in-orbit tests shown, it was concluded that the TEP's frequency response characteristic was not affected by launch, preinjection, or operating environments. The figure shows deviations in the frequency plots of 1.5 decibels peak to peak, which is attributed to frequency sensitivity errors of the power measurement device in the TEP. These deviations are not attributable to changes in the TEP. See section Radiofrequency Output Power for more-detailed information.

Data are presented for TEP operating band TB1 and for three constant drive levels. These three drive levels produce TEP output powers of saturation, saturation minus 3 decibels, and saturation minus 6 decibels center band.

Power-Out-versus-Power-In Tests

The transfer characteristics of the TEP were also measured and compared with previously taken ground data. Figure 34 shows a comparison between data taken before OST integration with the TEP, during thermal vacuum tests, and during in-orbit tests. The results show close agreement between in-orbit and ground data. The thermal vacuum tests were conducted under simulated in-orbit conditions. The system noise tends to decrease the magnitude of the slope of the P_{out}-versus-P_{in} plot at low input drive powers. Comparing this curve with the in-orbit curve, with no attenuators switched in either the TB1 or TB2 signal paths, shows similar characteristics at high input drive powers. The differences at the lower power levels are due to differences in the carrier-to-noise ratio. The difference in carrier-to-noise ratio is attributable to error in determining the free-path space loss and other atmospheric losses while testing in the thermal vacuum chamber. A plot of P_{out} versus P_{in} taken in orbit with a 5-decibel attenuator switched in the TB1 signal path shows greater similarity to bench

data taken before integration.

Figures 35 to 37 compare two different P_{out}-versus-P_{in} plots of 12.038, 12.080, and 12.123 gigahertz, respectively, taken during the first 3 months of in-orbit testing with the 5-decibel attenuator switched in the TB1 signal path. Within the resolution of the measurements, there is no change in the TEP transfer characteristic due to launch, preinjection, or operating environments. Because of discrepancies in the absolute level of output power, the P_{out}-versus-P_{in} plots were normalized. These discrepancies are discussed in the section Radiofrequency Output Power. The average output power at saturation in figure 35 is 54 dBm (decibels referred to milliwatts). In figure 36, the average saturated output power is 53.4 dBm; and in figure 37, it is 52.0 dBm. These output powers are consistent with data taken in thermal vacuum testing.

Output-Stage-Tube Nonlinearities

OST overdrive test. - An OST overdrive test was performed to experimentally determine the maximum OST overdrive operating condition, without actuating the body-current protection circuit in its operating environment, and to establish a basis for assessing possible changes in focusing. A single carrier at center band was amplified to produce saturation. After thermal stabilization was achieved, the uplink transmitter power was slowly increased until the body current was 9.1 milliamperes. Since the OST body-current protective shutdown point is set at 10.0 milliamperes, no attempt was made to further overdrive the OST.

The OST overdrive data obtained are shown in figure 38 and closely agree with data obtained during the OST thermal vacuum test. Slight differences between the ground and in-orbit tests (saturation plus 3.14 dB) are mainly due to the inability to precisely maintain the OST drive long enough to achieve thermal equilibrium. The OST drive perturbations attributable to the uplink antenna step-track update cycles were severe enough to cause OST high-voltage trips because of high body current.

Additional tests for the OST body-current sensitivity disclosed that the body current increased by approximately 10 percent over the normal value during amplification of extremely noisy signals. No difference in body current was detected when the carrier was frequency modulated up to standard video frequencies. The difference in body current between OST thermal vacuum tests and in-orbit tests at the 3.14-decibel overdrive condition (fig. 38) is attributed solely to the difference in OST body temperature.

AM-PM conversion test. - To characterize the CTS transponder/TEP system, the amplitude modulation - phase modulation (AM-PM) conversion coefficient was measured on the spacecraft for various OST output power conditions. For the transponder configuration used and the region of operation, the TEP is the largest contributor to AM-PM distortion. This can be seen by comparing OST ground test data (fig. 39). The

measurements were expected to be predominantly a representation of OST distortion characteristics.

The measurement was made by transmitting two unmodulated carriers separated by 1 megahertz (carrier 1 is 30 dB larger than carrier 2) to the spacecraft. The resulting OST output carrier ratios yielded the AM-PM coefficient (ref. 5). Close agreement was obtained between ground test and in-orbit data (fig. 39).

Intermodulation test. - Intermodulation performance measurements were conducted on the TEP by transmitting to the spacecraft two carriers separated by 10 megahertz. The downlink third-order intermodulation products were observed for carrier levels that produced conditions of saturation, saturation minus 3 decibels, saturation minus 6 decibels, and saturation minus 8 decibels from the OST.

For the transponder configuration used and the region of operation, the TEP is the largest contributor to the generation of intermodulation products. This can be seen by comparing OST ground test data (fig. 40). The measurements were expected to be predominantly a representation of OST intermodulation characteristics. No major changes between ground and in-orbit data were noted.

Gain suppression test. - To characterize the operation of the OST for dual-carrier operation, a gain suppression test was performed. This was accomplished by transmitting to the spacecraft two carriers separated by 40 megahertz. The OST was saturated with carrier 1 only (fig. 41), and the output power was monitored by telemetry and a spectrum analyzer. Carrier 2 output power was slowly increased while the OST rf output power of carrier 1 was monitored. Figure 41 shows the OST gain suppression characteristics. For dual-carrier operation, approximately 60 watts of rf power (5.2 dB below single-carrier saturation; saturation, 200 W) is contained in each carrier, with the remainder of the power in the intermodulation products.

Power Processing System Noise Test

This measurement was made to investigate the presence of PPS inverter frequencies and their harmonics in the received baseband signal and to establish a basis for future performance evaluation. A waveform analyzer was used to examine the baseband noise spectrum for an inverter frequency of 10 kilohertz and harmonic components. No measurable noise was observed. Test results are presented in table XIV.

SUMMARY OF RESULTS

Generalized results and observations developed from a series of thermal, communications, and electrical performance tests of the transmitter experiment package

(TEP) aboard the Communications Technology Satellite (CTS) during the first 90 days of spacecraft orbital operation are summarized in this section. The results represent 90 TEP operating days (out of 154 days in orbit) with a total of 1233 hours of TEP operation in orbit. The TEP was also operated for 1800 hours in prelaunch testing. The TEP consists of a nominal 200-watt output stage tube (OST), a supporting power processing system (PPS), and a variable-conductance heat pipe system (VCHPS). The thermal performance tests were performed at thermal equilibrium conditions in important TEP operating modes at several spacecraft orbital positions. The electrical performance tests were conducted to evaluate frequency response, radiofrequency (rf) output power, efficiency, and distortions. Communications tests were conducted with unmodulated carriers as well as with video- and audio-modulated signals. The results of the in-orbit tests were compared with ground test results.

DIRECT-CURRENT AND RADIOFREQUENCY PERFORMANCE

The TEP electrical performance characteristics in flight were compared with those observed during preflight thermal vacuum testing. Specifically, the following parameters were evaluated:

1. TEP efficiency: There has been no measurable change in the efficiency of either the PPS or the OST during space operation. While the measured values of OST efficiency were about 5 percent higher in space than they were in preflight testing, this difference is believed to be due to an uncertainty in the calibration of the output rf power measured on the spacecraft.

2. Output radiofrequency power: Output rf power measurements made at saturation during the first 90 days of space operation were essentially constant with time and were about 0.25 decibel higher than the measurements made in the preflight thermal vacuum tests. This difference is believed to be due to an uncertainty in the calibration of the output power sensor, which operates at a higher temperature in space ($\sim 25^{\circ}$ C higher) than it did during the ground tests.

3. Electron beam focusing: The consistency of body-current measurements at saturated OST rf output power conditions indicated that no change in electron beam focusing occurred during the first 90 days of TEP operation.

4. Cathode life: No measurable changes were observed in the beam-current data, which is an indication of sufficient cathode emission, during the flight testing period. Therefore, it was concluded that the cathode is operating normally and that there has been no change in its performance.

5. High-voltage space operation: No measurable leakage current across the TEP high-voltage insulators was observed during either the initial TEP turnon sequence or the second (posteclipse) turnon, which took place 75 days later.

6. OST internal pressure: The internal pressure of the OST remained essentially constant throughout the 90-day testing period.

THERMAL PERFORMANCE

The following thermal performance characteristics were evaluated:

1. Measured key TEP component temperatures remained well within the limits established for worst-case flight predictions at all operating conditions examined.

2. The OST and VCHPS temperatures are primarily influenced by TEP operating conditions, the spacecraft orbital position, and the Sun angle with the orbital plane. To a small extent, these temperatures are perturbed by minor variations, such as brief deviations in uplink (to spacecraft) transmitted power level and/or frequency and changes in atmospheric conditions and ground antenna-pointing cycles.

3. Typical OST and VCHPS temperatures or ranges of temperature have been established for the various operating conditions examined in this study. Significant departures from these typical ranges may indicate OST and/or VCHPS performance changes.

4. Approximately 2 hours was required for the OST to achieve essential thermal equilibrium after an operating condition change. The TEP rf performance was normal throughout an OST thermal transient period.

5. No measurable evidence of OST thermal performance change was observed during this investigation. Within the limits of measurement accuracy, OST temperatures exhibited excellent repeatability for similar operating conditions.

6. The VCHPS functioned thermally as designed throughout the testing period of this study, turning on and off as required to maintain the temperatures of the TEP components within safe prescribed limits. Specifically, the PPS baseplate temperature was maintained below 50° C at all times.

COMMUNICATIONS PERFORMANCE

The spacecraft test results were compared with results of preflight thermal vacuum tests of the transponder/TEP system. The flight test data indicate that no significant changes in TEP communications performance characteristics occurred during the first 90 days of spacecraft operation. Specifically, the following parameters were evaluated:

1. Overdrive operation: Overdrive characteristics were essentially identical to those observed in preflight thermal vacuum testing. Small differences were due to drive-level perturbations caused by ground antenna update cycles and to differences in OST body temperature between flight and preflight test conditions.

2. AM-PM conversion: Very small differences in the amplitude modulation - phase modulation conversion coefficient, relative to preflight data, were recorded only at OST drive levels of 8 decibels below saturation and lower. The noise level and measurement error become significant at this low drive level.

3. Gain suppression characteristics: Dual-carrier operation characteristics of the TEP in orbit were unchanged from those observed in preflight testing.

4. PPS inverter noise effects: No measurable noise was observed in the ground-received baseband that was attributable to the PPS inverter noise.

5. Intermodulation characteristics, video signal-to-noise ratio, differential phase characteristics, differential gain characteristics, frequency response characteristics, and power transfer characteristics: No significant changes in these flight characteristics relative to those recorded in preflight testing were observed.

Lewis Research Center,
National Aeronautics and Space Administration,
Cleveland, Ohio, April 26, 1977,
610-22.

REFERENCES

1. Alexovich, R. E.: The 200 Watt SHF Transmitter Experiment Package. NASA TM X-68106, 1972.

2. Kosmahl, Henry G.: A Novel, Axisymmetric, Electrostatic Collector for Linear Beam Microwave Tubes. NASA TN D-6093, 1971.

3. Chomos, Gerald J.; and Curren, Arthur N.: Description and Expected Performance of Flight-Model, 12-Gigahertz, Output Stage Tube for the Communications Technology Satellite. NASA TM X-3441, 1976.

4. In-Service Random Noise Measurements Using the Tektronix 147. Application Notes No. 3. Television Products Engineering. Tektronix, Inc.

5. Laico, J. P.; McDowell, H. C.; and Master, C. R.: A Medium-Power Traveling-Wave Tube for 6000-Mc Radio Relay. Bell System Technical J., vol. 35, Nov. 1956, pp. 1285-1346.

TABLE I. - POWER-PROCESSING-SYSTEM PERFORMANCE CHARACTERISTICS

Converts 28-V and 76-V dc power to -
Nine high-voltage collector supplies (cathode voltage, -11.3 kV; current, 72 mA; regulation, ±1 percent; ripple, 0.01 percent)
Cathode heater supply (voltage, 4.2 V; current, 1.5 A; floating at -11.3 kV)
Anode supply (voltage, 350 V ± 200 V; current, 100 mA)
Ion pump supply (voltage, 4 kV; current, 50 μA)
Protects system against -
Excessive current in output stage tube
Excessive pressure in output stage tube
Excessive arcing
High or low voltage on input lines (tolerates 95 and 45 V)
Power conversion efficiency, 86.56 percent to 88.51 percent

TABLE II. - TRANSMITTER-EXPERIMENT-PACKAGE TELEMETRY DATA SUMMARY

Cathode heater voltage, V dc	0 - 10
Cathode voltage, kV	0 - -15
Beam current, mA	0 - 100
Output-stage-tube body current, mA	0 - 15
Anode voltage, V dc	0 - 600
Collector voltages (3), kV	0 - -10
Collector currents (10), mA	0 - 40
Output-stage-tube and power-processing-system temperatures, ^{o}C (^{o}F)	-55 - 225 (-65 - 435)
Radiofrequency power (2), W	0 - 250
Output-stage-tube internal pressure, N/m^2 (torr)	1.33×10^{-4} - 1.33×10^{-6} (10^{-6} - 10^{-8})
Bus currents, A	0 - 10
Heat-pipe temperatures (6), ^{o}C (^{o}F)	-73 - 93 (-100 - 200)

TABLE III. - POWER-PROCESSING-

SYSTEM COMMAND LIST

Command	Description
1	Special instrumentation on
2	Power-processing-system enable
3	Protection on and fault telemetry reset
4	High-voltage protection on
5	Substitute heaters off
6	Cathode heater off (substitute heaters on)
7	Anode and cathode collector on
8	Anode and cathode collector off
9	Cathode heater at 50-percent power
10	Cathode heater at 100-percent power
11	Cathode heater at 110-percent power
12	Cathode heater at 120-percent power
13	Power-processing-system disable
14	All instrumentation off
15	Excessive pressure protection defeat
16	Excessive body-current protection defeat
17	High-voltage protection defeat
18	Close transmitter-experiment-package 76-volt bus switch
19	Open transmitter-experiment-package 76-volt bus switch
20	Preregulator bypass

TABLE IV. - OUTPUT-STAGE-TUBE

PERFORMANCE SPECIFICATIONS

Nominal radiofrequency output power, W	200
Efficiency goal, percent	50
Center-band frequency, GHz	12.0805
Bandwidth (3 dB), MHz:	
Minimum	85
Maximum	250
Saturated gain, dB	30
Small signal gain variation (peak to peak), dB	5
Second-order phase deviation, deg/MHz^2	0.2
Noise figure, dB	40

TABLE V. - SUPER-HIGH-FREQUENCY GROUND-STATION CHARACTERISTICS

Location:	
Area	Lewis Research Center, Cleveland, Ohio
Latitude	$41^{\circ}24'45''$ N
Longitude	$81^{\circ}51'55''$ W
Elevation, m (ft)	231 (758)
Antenna:	
Type	Parabolic reflector with Cassegrain feed
Diameter, m (ft)	5 (16)
Polarization	Linear orthogonal (transmit/receive)
Mount	Elevation over azimuth
Receiving frequency	11.983 GHz ± 150 MHz (11.7-GHz beacon)
Transmitting frequency	14.150 GHz ± 150 MHz
Gain to temperature ratio, dB	23.5
Gain (receive), dB	53.0
Gain (transmit), dB	54.4
Receiving system noise temperature, K	800
Effective isotropic radiated power (EIRP), dBW	85
Beam width (3 dB), deg:	
Receive	0.37
Transmit	0.32
Tracking accuracy (step track), deg	±0.05
Transmitter:	
Frequency, GHz	14
Modulation	FM
Maximum power output, kW	1.25
Radiofrequency bandwidth, MHz	85
Modulators (two each):	
Frequency, GHz	14
Modulation	FM
Power output, dBm	22.6
Subcarriers (audio), MHz	7.5, 5.14, 5.41, 5.79
Preemphasis:	
Video	CCIR
Audio, μsec	75
Deviations (peak to peak):	
Video, MHz	10 - 30
Carrier by subcarrier, MHz	1.98
Subcarrier by audio, kHz	120 - 200
Demodulators (two each)[a]:	
Frequency, GHz	12
Modulation	FM

[a]Compatible with modulators, except for frequency.

TABLE VI. - SUPER-HIGH-FREQUENCY GROUND-STATION SAMPLE UPLINK CALCULATION

	Transponder gain, dB	
	125	120
Uplink frequency, GHz	14.2	14.2
Terminal transmitter power (171.7 W, 543 W), dBW	22.35	27.35
Terminal feed loss, dB	-3.00	-3.00
Terminal antenna gain (5-m (16-ft) diam; 0.31° half-power beam width), dB	54.53	54.53
Terminal effective isotropic radiated power, dBW	73.88	73.88
Terminal antenna stationkeeping loss (0°), dB	-0	-0
Terminal antenna pointing error (0.05°), dB	-0.26	-0.26
Margin, dB	-3.00	-3.00
Propagation loss (altitude, 38 531 km (23 974 mi); latitude, 41.4° N; relative longitude, 35.1°), dB	-207.22	-207.22
Atmospheric loss (0.1-percent outage; CCIR rainfall region 2), dB	-2.23	-2.23
Polarization loss, dB	-0.25	-0.25
Spacecraft feed loss, dB	-0.50	-0.50
Spacecraft antenna gain (0.81-m by 0.81-m (2.7-ft by 2.7-ft) diam; 2° by 2° half-power beam width)	37.90	37.90
Spacecraft antenna beam-edge loss, dB	-0	-0
Spacecraft antenna pointing error (0.38°), dB	-0.32	-0.32
Spacecraft received carrier power, dBW	-102.00	-97.00
Spacecraft noise power density (1315 K), dBW/Hz	-191.41	-197.41
Bandwidth (27 MHz), dB (Hz)	74.31	74.31
Spacecraft receiver noise power, dBW	-123.10	-123.10
Spacecraft carrier-to-noise ratio, dB	21.10	26.10

TABLE VII. - SUPER-HIGH-FREQUENCY GROUND-STATION

SAMPLE DOWNLINK CALCULATION

	Transponder gain, dB	
	125	120
Downlink frequency, GHz	12.1	12.1
Spacecraft output-stage-tube power (200 W), dBW	23.01	23.01
Spacecraft feed loss, dB	-0.85	-0.85
Spacecraft antenna gain (0.81-m by 0.81-m (2.7-ft by 2.7-ft) diam; 2.35° by 2.35° half-power beam width), dB	36.90	36.90
Spacecraft effective isotropic radiated power, dBW	59.06	59.06
Spacecraft antenna beam-edge loss, dB	-0	-0
Spacecraft antenna pointing error (0.35°), dB	-0.22	-0.22
Margin, dB	-3.00	-3.00
Propagation loss (altitude, 38 581 km (23 974 mi); latitude, 41.4° N; relative longitude, 35.1°), dB	-205.81	-205.81
Atmospheric loss (0.1-percent outage; CCIR rainfall region 2), dB	-1.52	-1.52
Polarization loss, dB	-0.25	-0.25
Terminal feed loss, dB	-1.00	-1.00
Terminal antenna gain (5-m (16-ft) diam; 0.36° half-power beam width), dB	53.12	53.12
Terminal antenna stationkeeping loss (0°), dB	-0	-0
Terminal antenna pointing error (0.05°), dB	-0.18	-0.18
Terminal received carrier power, dBW	-99.80	-99.80
Terminal noise power density (800 K), dBW/Hz	-199.57	-199.57
Bandwidth (40 MHz), dB (Hz)	76.02	76.02
Terminal receiver noise, dBW	-123.55	-123.55
Uplink noise contribution (uplink carrier-to-noise ratios of 21.1 dB and 26.1 dB, respectively), dB	5.71	2.70
Terminal net noise power, dBW	-117.84	-120.85
Terminal carrier-power-to-receiver-noise ratio, dB	18.04	21.05
Frequency-modulation improvement (modulation index 2), dB	21.58	21.58
Noise weighting factor (CCIR), dB	10.20	10.20
Pre- and deemphasis improvement, dB	2.40	2.40
Signal-to-noise ratio, dB	52.22	55.23

TABLE VIII. - UPLINK AND DOWNLINK

SIGNAL EXPERIENCE

[Downlink TB2 at zero radiofrequency power; all data obtained at center-band downlink TB1; modulation index 2.]

Attenuator 2, dB	Uplink effective isotropic radiated power[a] (to saturate OST), dBW		Downlink signal-to-noise ratio[c] (at OST saturation), dB	
	Minimum predicted[b]	Actual	Optimum predicted	Actual
0	66.7	68.5	57.0	53.2
5	71.7	73.5	60.0	56.2

[a] $P_{xtr} - L_{FEED} + G_{ANT}$.

[b] Excludes all margin, rain attenuation, and antenna pointing errors.

[c] CCIR weighted; measuring accuracy, ±1 dB.

TABLE IX. - SUPER-HIGH-FREQUENCY TRANSMITTER EXPERIMENT PACKAGE MEASUREMENT AND TESTING SCHEDULE

Date 1976	Current offset calibration	Quick turnon	Ratio of power in to power out	Efficiency	Frequency response	Single- and dual-channel video	Audio response	PPS noise	Multi-channel telephony	Gain support	AM-PM conversion	Intermodulation	Overdrive	Thermal stability
Feb. 8	•	•	•	•	•	•								
9			•	•	•						•		•	•
10			•	•	•	•		•					•	•
11						•								•
12			•	•	•	•				•				•
13			•	•	•				•					•
14						•					•			•
15			•			•	•					•		•
16			•	•	•	•				•				•
17														•
24	•		•	•	•			•						•
25											•			•
Mar. 2			•	•	•									
3														•
No communications operations														
Apr. 24	•		•	•	•									
May 4	•		•	•	•						•			•
5	•							•	•	•		•		•
8	•					•								•
9			•											•
10				•	•									•
12	•					•								•
17	•		•											
18				•	•									•
21	•													
22														•
23	•		•			•	•							•
24	•													•
25														•
28	•			•	•									•
29														•
31	•		•	•	•									•
June 4	•											•		•
5														•
6	•		•	•	•						•			•
7														•
9	•													
10														•
11	•													•
12														•
13			•	•	•						•	•		•

TABLE X. - POWER-PROCESSING-SYSTEM ELECTRICAL CHARACTERISTICS AND EFFICIENCY FOR SELECTED OPERATING PERIODS

Day in orbit	Time	Experiment array voltage, V	Experiment array current, A	Power-processing-system baseplate temperature, ^{o}C	Power to output stage tube, W	Power from solar array, W	Power-processing-system efficiency, percent
40	1539:40	82.89	5.51	41.7	409.67	473.26	86.56
40	2138:20	82.89	6.21	42.8	464.05	531.63	87.29
41	0339:30	82.89	6.23	46.1	467.18	533.27	87.61
43	2343:19	82.89	6.20	47.2	463.52	530.20	87.42
44	1720:57	82.30	6.19	38.3	464.26	525.78	88.30
45	0116:08	82.30	6.38	48.9	475.32	541.70	87.75
45	0917:55	82.30	6.19	45.6	465.33	525.72	88.51
45	1721:40	82.30	6.48	44.4	480.13	550.30	87.25
46	1514:00	82.30	6.20	41.1	461.49	527.14	87.55
47	0734:40	82.30	6.14	44.4	460.18	521.59	88.23
48	0319:10	82.89	5.43	42.8	410.01	466.57	87.88
55	1539:50	81.71	6.28	40.0	466.70	530.05	88.05
56	1545:37	81.71	6.32	39.4	469.04	533.34	87.94
63	1019:10	82.30	6.21	41.7	466.51	527.41	88.45
115	2115:00	82.30	6.21	35.6	465.13	528.01	88.09
125	1039:37	82.89	6.24	39.4	472.60	533.60	88.57
125	2209:23	82.89	6.07	33.3	459.45	519.75	88.40
126	1054:50	82.89	5.44	36.7	410.79	467.18	87.93
126	2239:40	83.49	5.12	34.4	386.33	443.82	87.05
130	2239:46	82.89	6.57	37.2	492.79	561.42	87.78
131	0446:13	82.89	6.30	47.8	471.23	538.86	87.45
133	1039:40	82.89	6.15	40.0	461.67	526.65	87.66
134	0439:30	82.89	6.39	43.3	475.80	546.36	87.09
139	0439:22	83.49	5.35	37.2	405.00	463.39	87.40

TABLE XI. - EQUILIBRIUM THERMAL OUTPUT-STAGE-TUBE AND VARIABLE-CONDUCTANCE HEAT PIPE SYSTEM CHARACTERISTICS

Radiofrequency output	Operating frequency	Transmitter-experiment-package input power (typ.), W	Body current (typ.), mA	Output-stage-tube efficiency (typ.), percent	Temperature range (low to high), [b] °C				
					BODY	CPLR	MCD1	MDC2	HP1T
Saturation (typ. 245 W)	Center band	460	6.5	53	52 - 62	73 - 84	138 - 182	65 - 76	29 - 41
Saturation (typ. 150 W)	Upper band edge	405	5.5	37	50 - 57	70 - 76	142 - 159	62 - 67	29 - 39
Saturation (typ. 213 W)	Lower band edge	480	5.7	39	50 - 60	76 - 86	146 - 185	65 - 74	29 - 39
~100 W (nom. saturation minus 3 dB)	Center band	300	2.4	34	39 - 48	52 - 61	160 - 196	52 - 64	25 - 35
	Upper band edge	300	2.8	31	46 - 47	56 - 58	156 - 157	55 - 56	33 - 35
	Lower band edge	315	2.3	34	39 - 46	53 - 58	160 - 172	52 - 59	25 - 35
~0 W (direct-current beam)	(c)	175	1.7	(c)	35 - 40	33 - 41	160 - 196	40 - 53	-12 - 33

[a]Center band, 12.080 GHz; upper band edge, 12.123 GHz; lower band edge, 12.038 GHz.

[b]Refer to text for instrument descriptions.

[c]Not applicable.

TABLE XII. - SUBJECTIVE VIDEO

INTERFERENCE RATING SCALE

Interference perceptibility	Interference objectionableness
Imperceptible	Not annoying
Barely perceptible	Slightly annoying
Definitely perceptible	Definitely annoying
Very perceptible, but picture content ascertainable	Very annoying
Picture content impossible to ascertain	Extremely annoying

TABLE XIII. - SINGLE-CHANNEL VIDEO TEST SUMMARY

[Ground-station video system characteristics to point of measurement, differential phase, 0.7°; differential gain, 1.5 percent; signal-to-noise ratio, 58 dB.]

Frequency, GHz	Quantity	Output-stage-tube operating point relative to saturation, dB						
		+3	+2	+1	0	-1	-2	-3
12.059	Differential phase, deg	4	4	2	4	3	4	2
	Differential gain, percent	4	3	3	2	5	4	2
	Signal-to-noise ratio (unweighted)	48	47	47	47	46	44	43
12.080	Differential phase, deg	4.5	4	4	4	4.5	4.5	4.5
	Differential gain, percent	3	4	4	4	4	4	4
	Signal-to-noise ratio (unweighted)	47	47	46	45	45	44	42
12.101	Differential phase, deg	4	4	4	4.5	4.5	4.5	4.5
	Differential gain, percent	4	4	4	4	4	4	4
	Signal-to-noise ratio (unweighted)	46	47	46	46	45	43	41

TABLE XIV. - MULTICHANNEL TELEPHONE TEST SUMMARY

Telephone channels	Baseband frequency, kHz	Transmitter-experiment-package operating point	Uplink frequency, GHz			
			14.226		14.2685	
			Absolute noise power,	Decibels above reference noise, dBrnc	Absolute noise power,	Decibels above reference noise, dBrnc
60	70	Saturation plus	1.3×10^{2}	19.4	2.5×10^{1}	12.26
	270	2 dB	5.0×10^{1}	15.3	1.6×10^{1}	10.32
	70	Saturation	5.0×10^{2}	25.3	5.0×10^{11}	15.27
	270		1.6×10^{2}	20.3	3.2×10^{1}	13.33
	70	Saturation minus	1.0×10^{4}	38.3	7.9×10^{2}	27.25
	270	6 dB	2.5×10^{3}	32.3	3.2×10^{2}	23.33
960	70	Saturation plus	1.6×10^{2}	20.3	2.5×10^{1}	12.26
	1248	2 dB	5.0×10^{1}	15.3	3.2×10^{1}	13.33
	3886		4.0×10^{2}	24.3	2.0×10^{2}	21.29
	70	Saturation	4.0×10^{2}	24.3	5.0×10^{1}	15.27
	1248		1.0×10^{2}	18.3	5.0×10^{1}	15.27
	3888		6.3×10^{2}	26.3	4.0×10^{2}	24.30
	70	Saturation minus	7.9×10^{3}	37.3	7.9×10^{2}	27.25
	1248	6 dB	7.9×10^{2}	27.3	2.5×10^{2}	22.26
	3886		2.0×10^{3}	31.3	2.0×10^{3}	31.29

TABLE XV. - RECEIVED BASEBAND

INVERTER NOISE

[Reference saturation, -3 dBm at 3.77 MHz (modulation index, 2).]

Output-stage-tube operating point	Inverter frequency, kHz				
	10	20	30	40	50
	Received baseband inverter noise, dBm				
Saturation (continuous wave)	-80	-84	-80	-84	-85
Saturation minus 10 dB (continuous wave)	-60	-60	-60	-60	-60

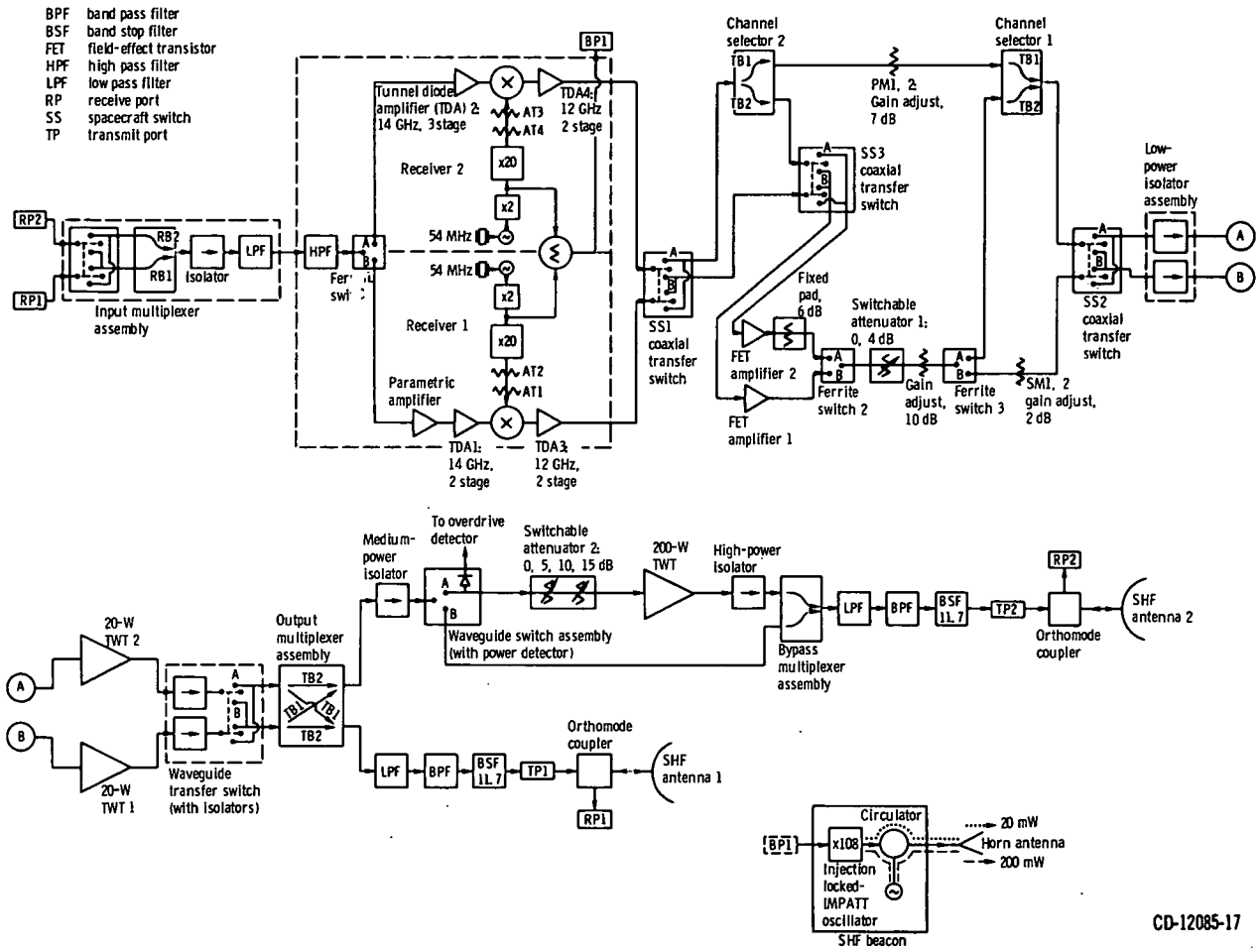

Figure 1. - Block diagram of super-high-frequency transponder.

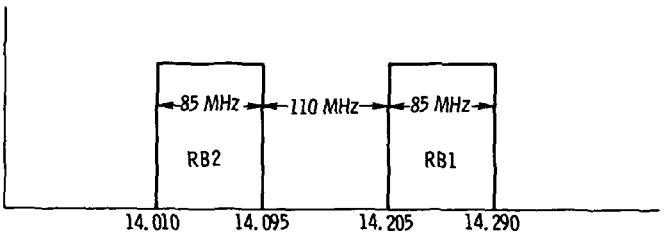

(a) Receive band.

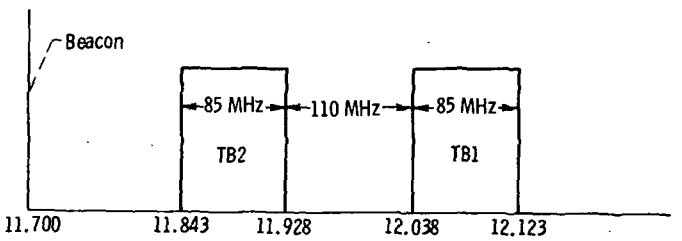

(b) Transmit band.

Figure 2. - Transponder frequency plan.

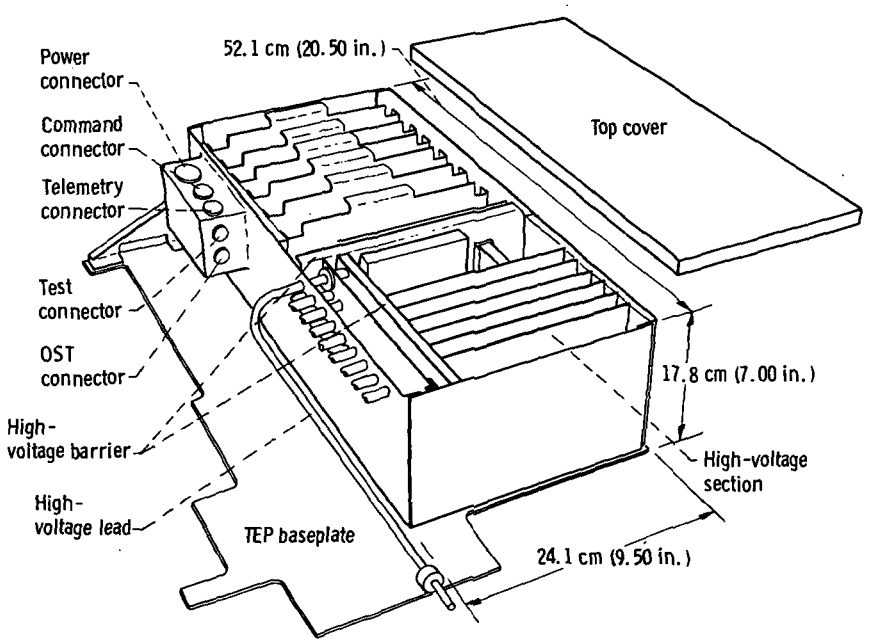

Figure 3. - Power-processing-system physical dimensions.

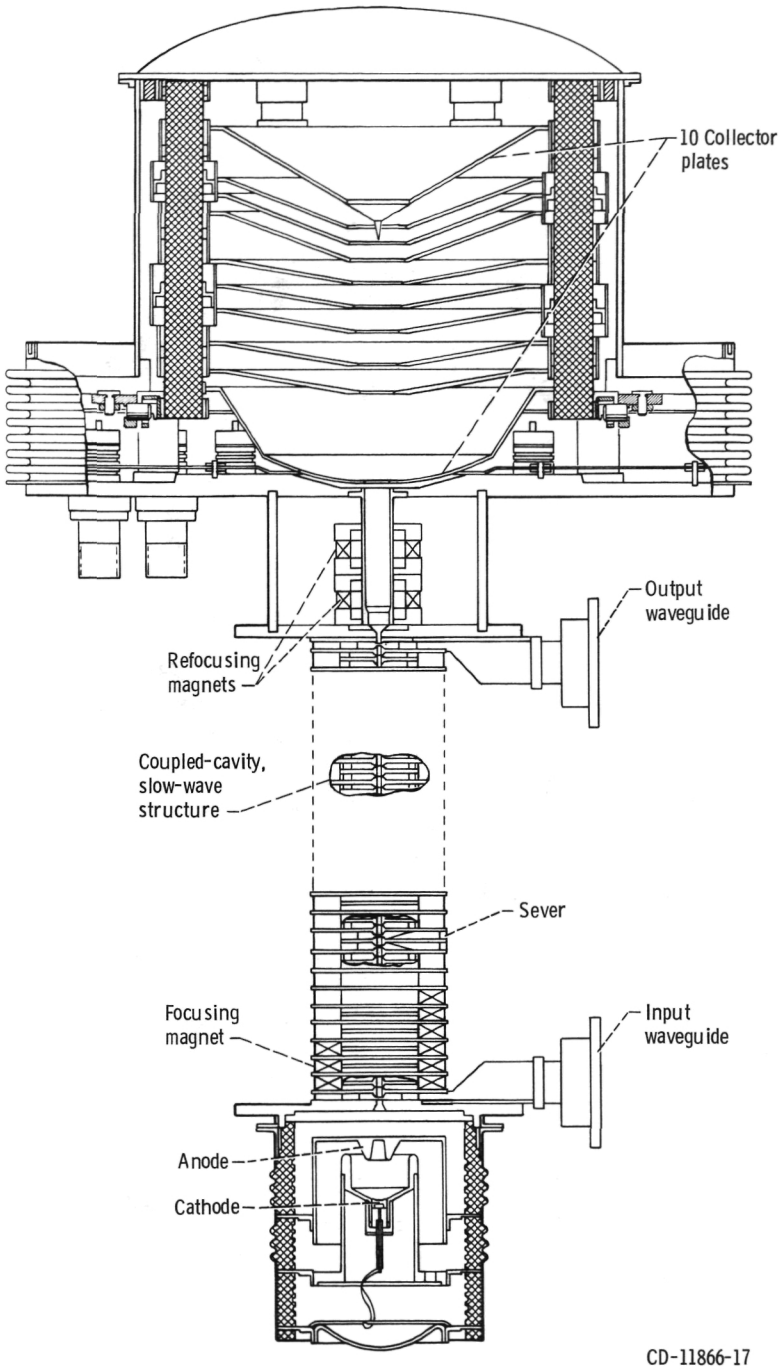

Figure 4. - Coupled-cavity, traveling-wave tube with multistage depressed collector.

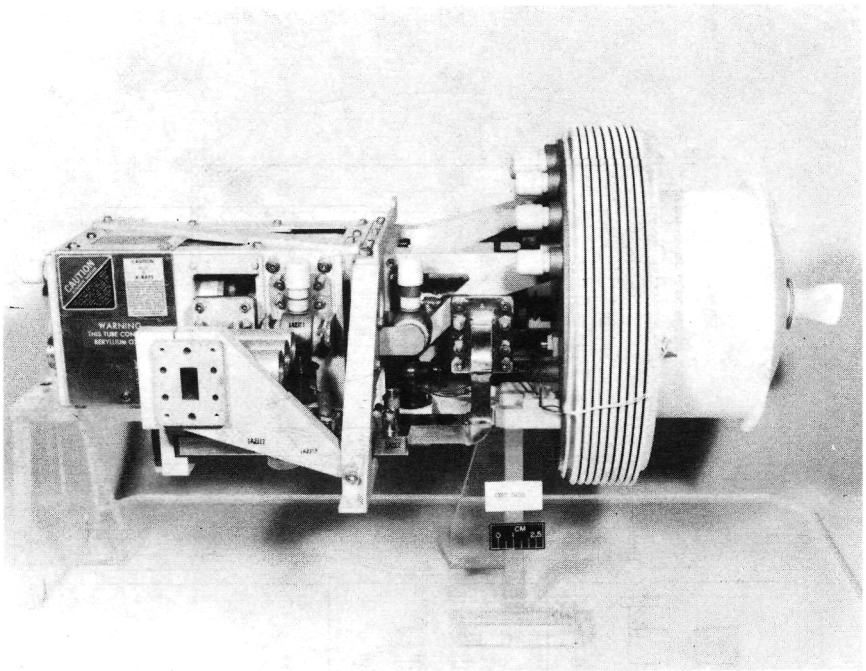

Figure 5. - Output stage tube.

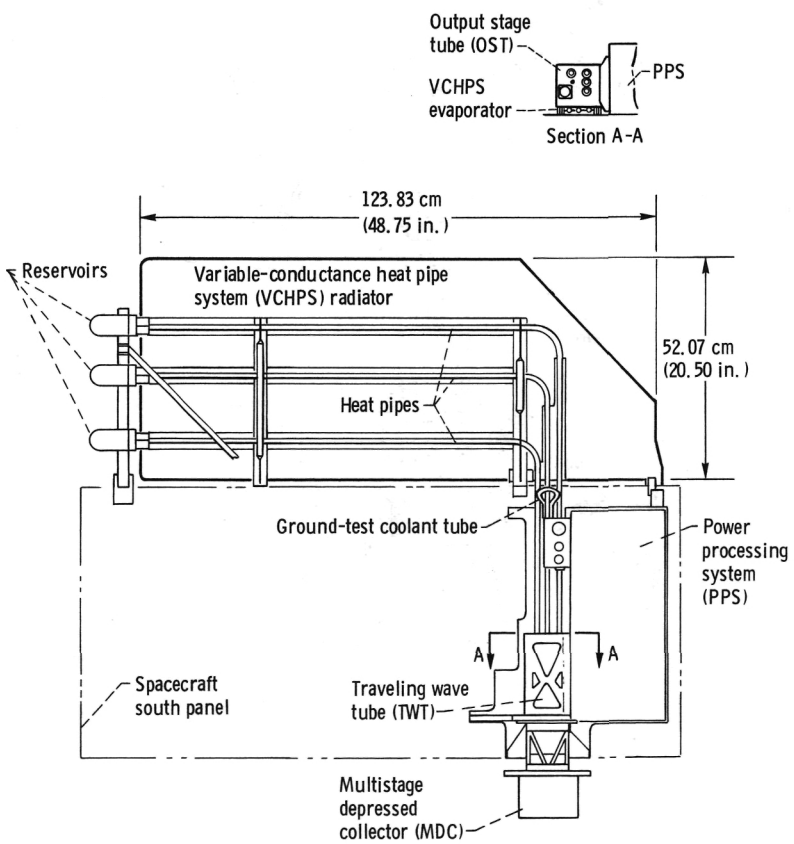

Figure 6. - Transmitter experiment package and variable-conductance heat pipe subsystem.

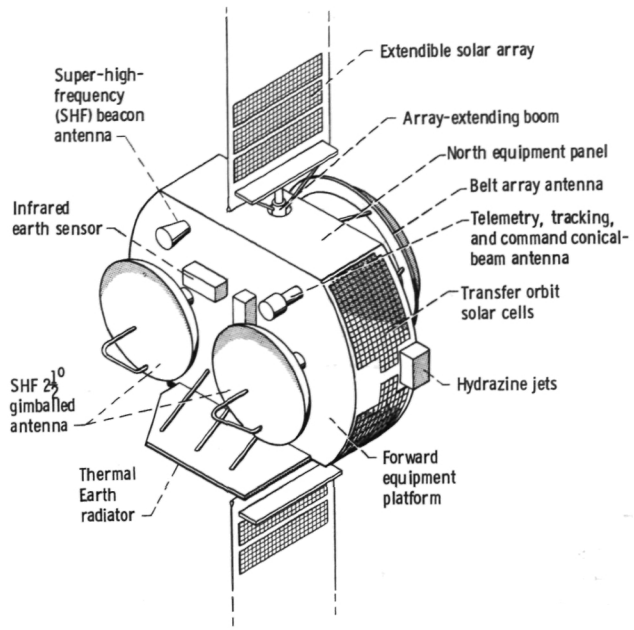

Figure 7. - View of CTS from Earth-viewing direction.

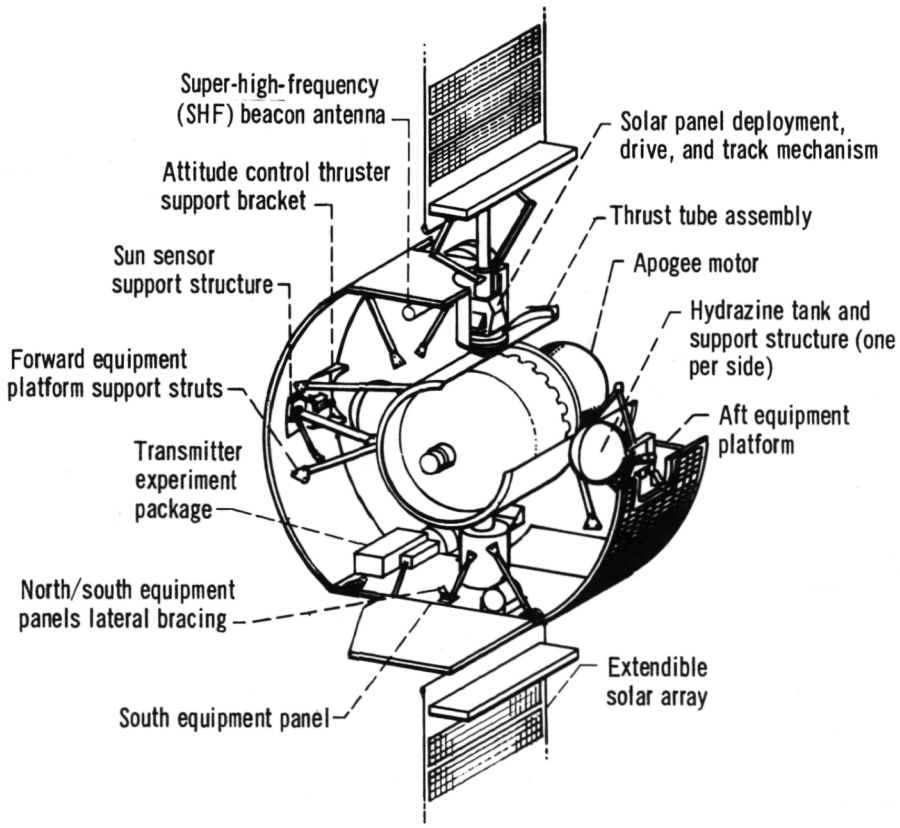

Figure 8. - View of CTS with forward platform and thermal shields removed.

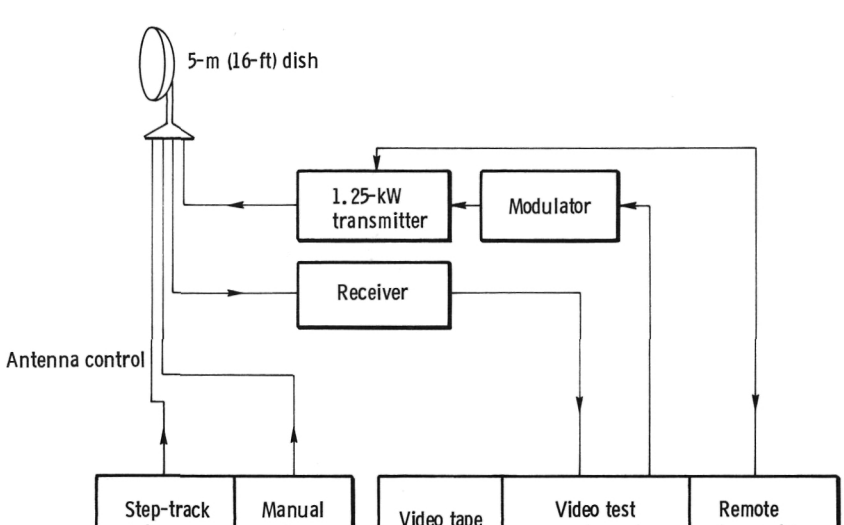

Figure 9. - Super-high-frequency ground-station arrangement.

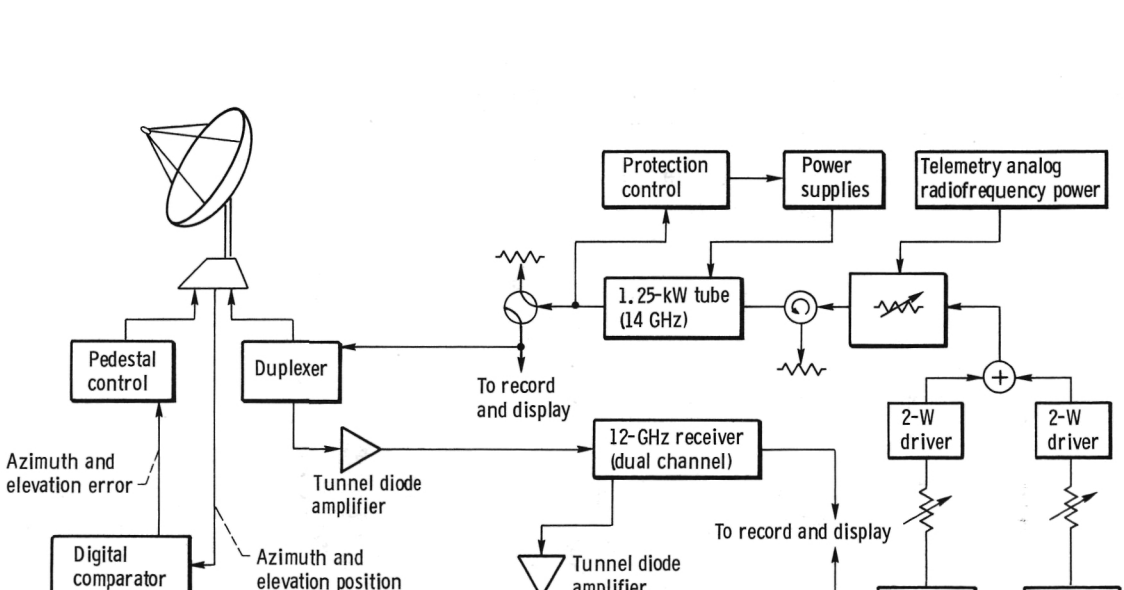

Figure 10. - Super-high-frequency ground-station block diagram. Antenna transmit gain (14 GHz), 54.4 dB; antenna receiver gain (12 GHz), 53.0 dB; beam width at 14 GHz, 0.32^{0}; beam width at 12 GHz, 0.37^{0}; antenna diameter, 5 m (16 ft).

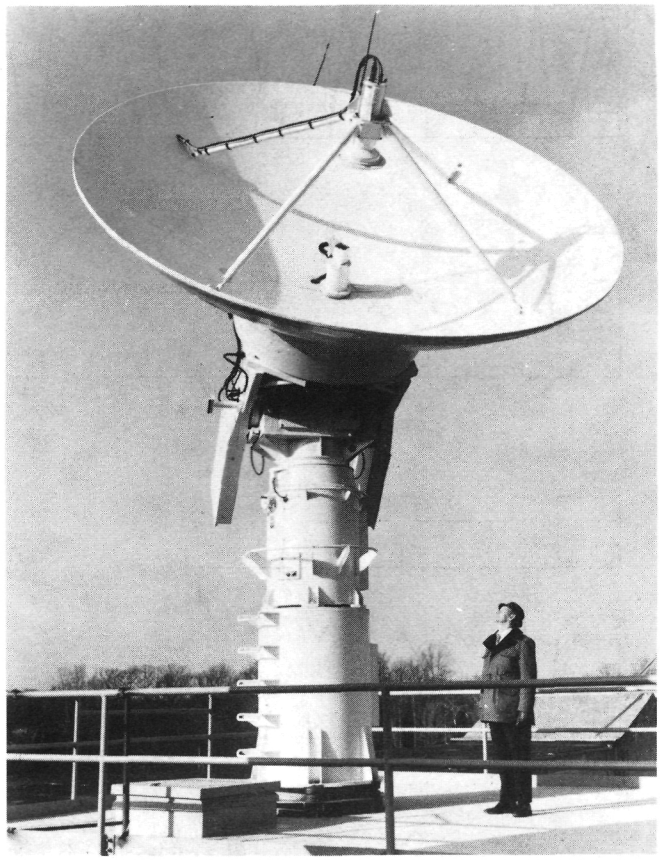

Figure 11. - Five-meter-diameter (16-ft) super-high-frequency Cassegrain antenna.

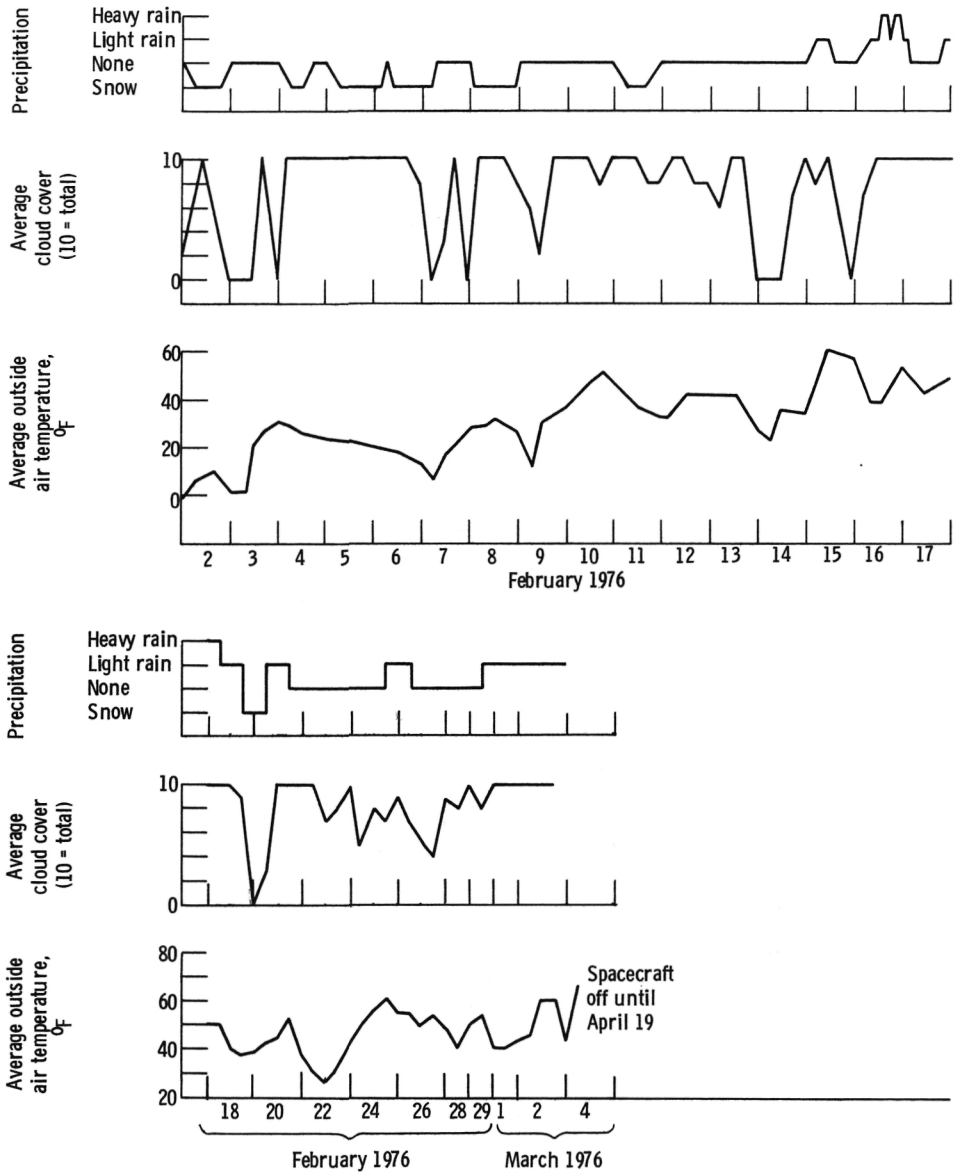

Figure 12. - Environmental conditions for period. Supplied by National Weather Service, Cleveland Hopkins Airport.

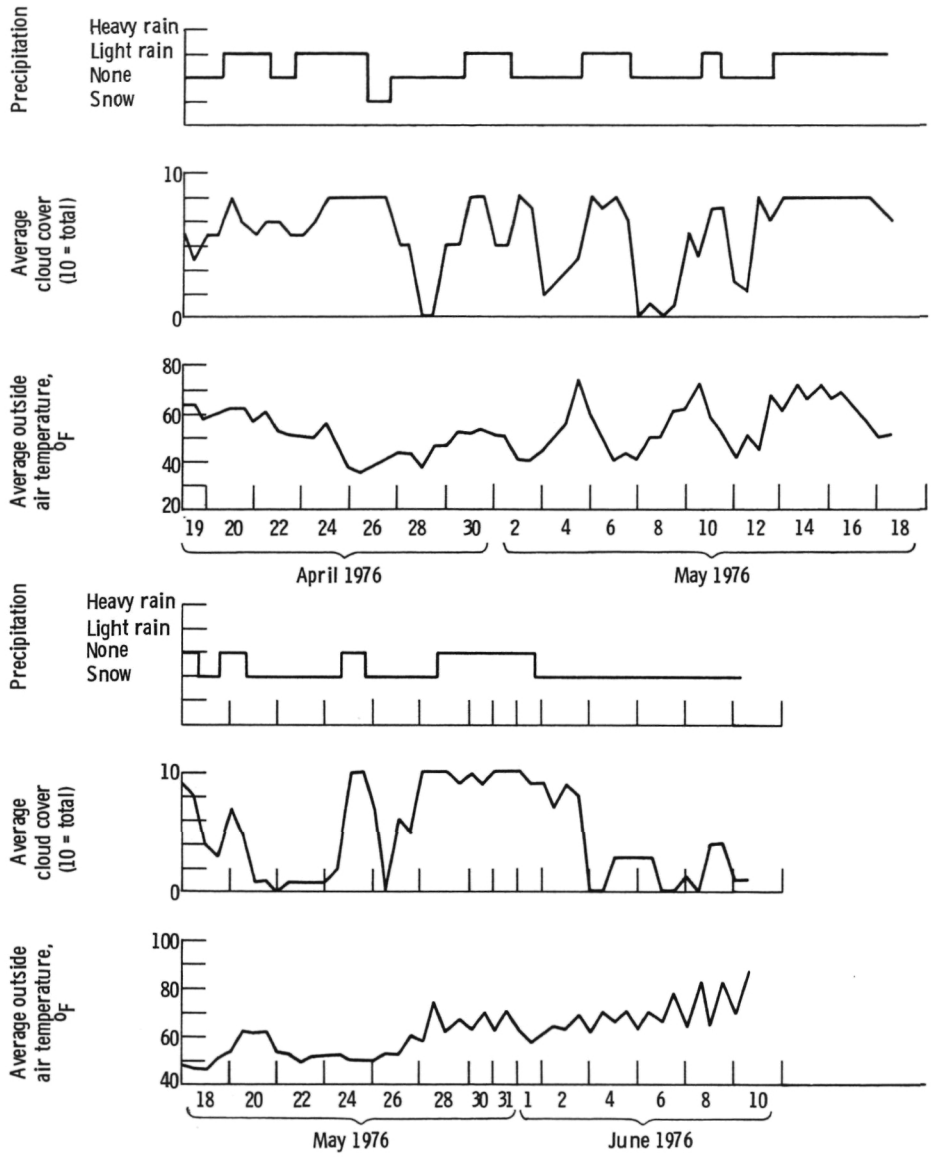

Figure 12. - Concluded.

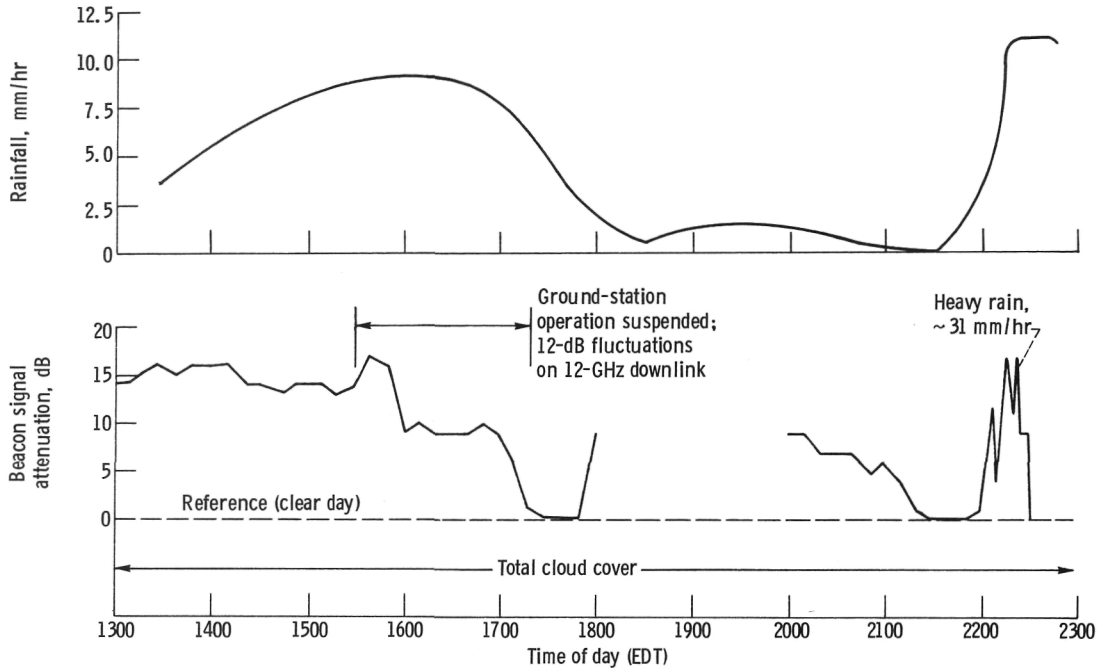

Figure 13. - CTS beacon signal attenuation (11.7 GHz) at Lewis ground station on February 16, 1976. (Rain rate recorded by National Weather Service, Cleveland Hopkins Airport, approx. 3 km (2 miles) from Lewis ground station.)

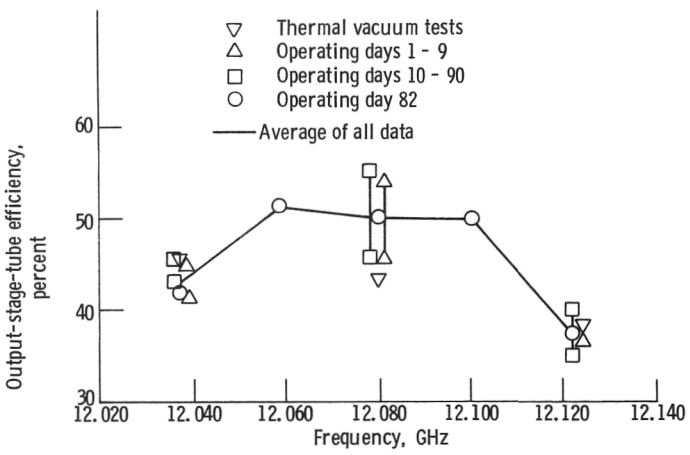

Figure 14. - Output-stage-tube overall efficiency at saturated output power as function of frequency.

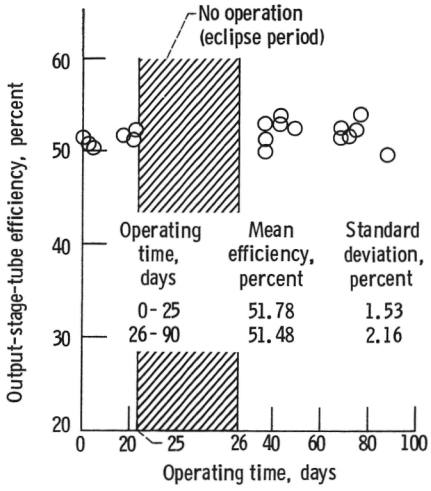

Figure 15. - Output-stage-tube overall efficiency at saturated output power as function of output-stage-tube operating time. Frequency, 12.080 GHz.

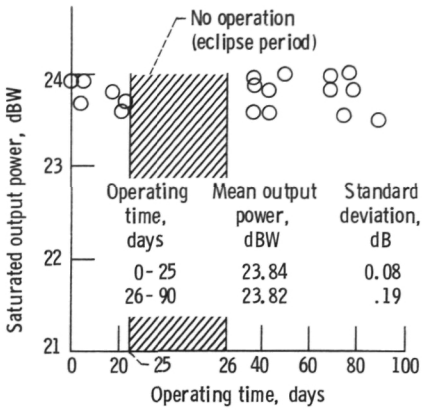

Figure 16. - Output-stage-tube radio-frequency output power as function of time. Frequency, 12.080 GHz.

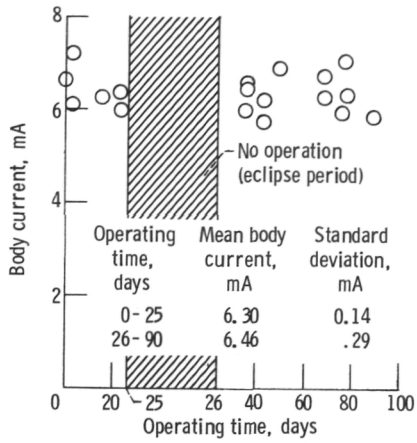

Figure 17. - Output-stage-tube body current at saturated output power as function of time. Frequency, 12.080 GHz.

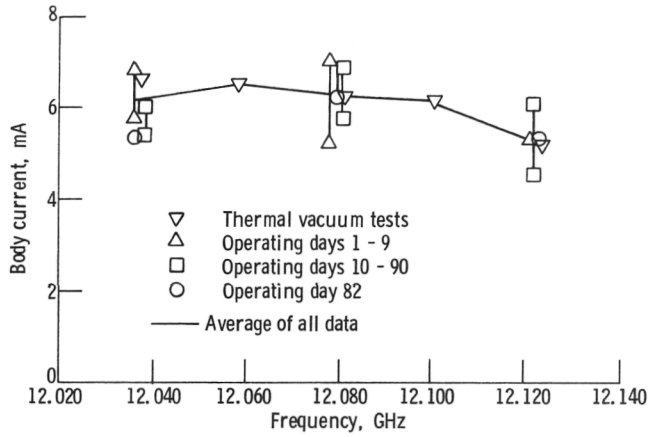

Figure 18. - Output-stage-tube body current at saturated output power as function of frequency.

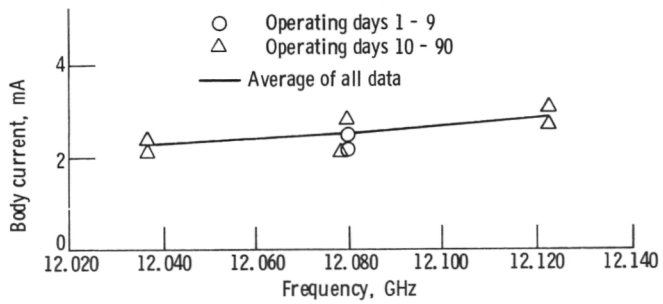

Figure 19. - Output-stage-tube body current at 100-watt output power as function of frequency.

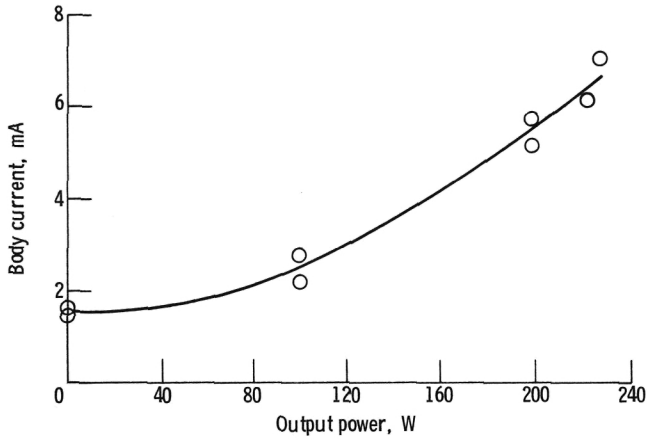

Figure 20. - Output-stage-tube body current at thermal stability as function of output power. Frequency, 12.080 GHz.

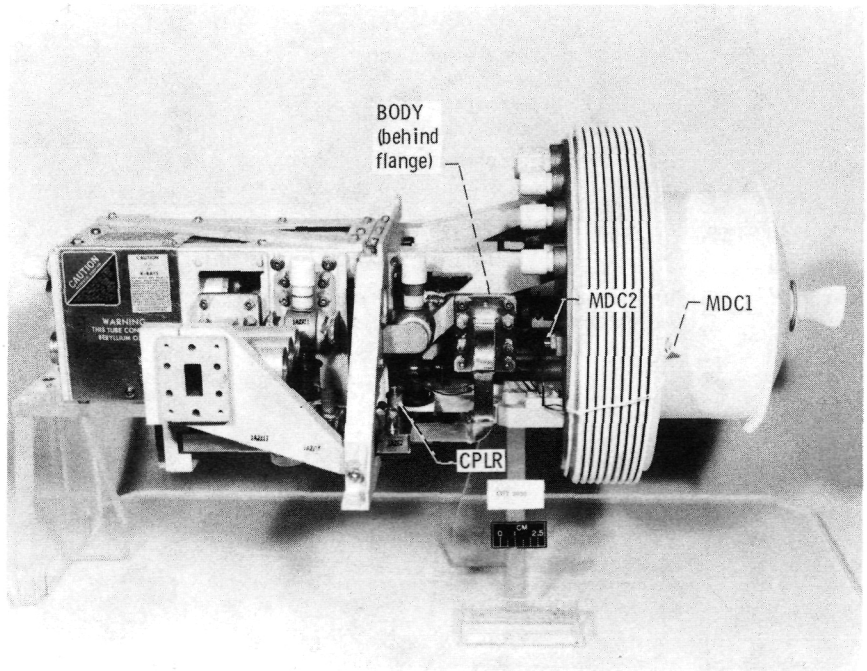

Figure 21. - Output stage tube, showing thermal instrumentation.

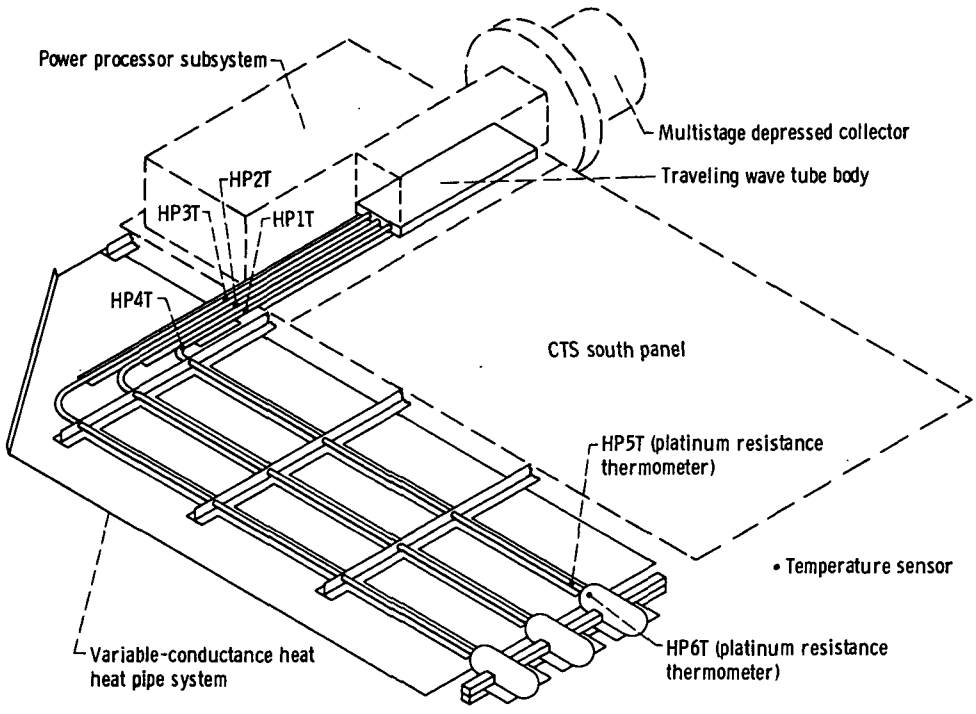

Figure 22. - Schematic of variable-conductance heat pipe subsystem, showing temperature sensor locations.

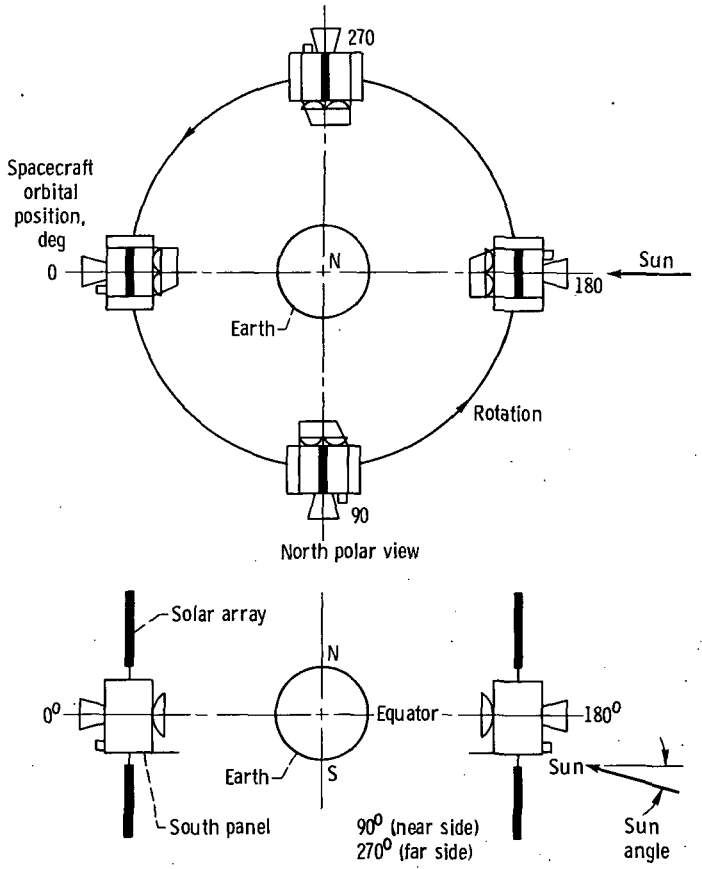

Figure 23. - Spacecraft orbital positions.

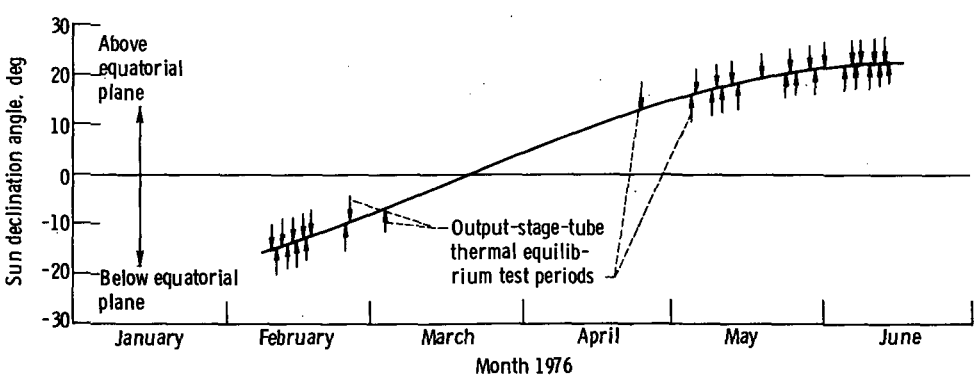

Figure 24. - Sun angle relative to equatorial plane (declination angle) at CTS spacecraft noon position (180° orbital position) as function of date.

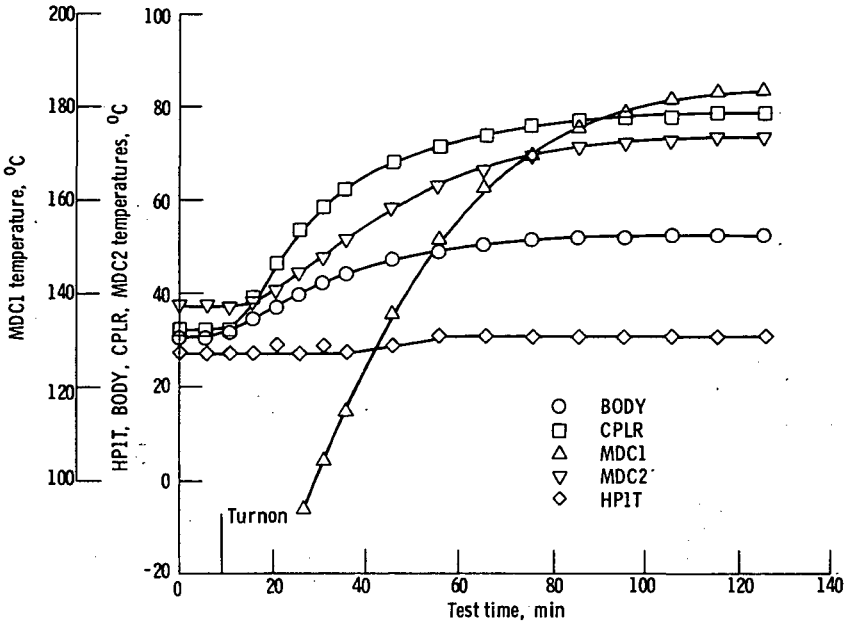

Figure 25. - Several output-stage-tube and variable-conductance heat pipe system temperatures during an output-stage-tube thermal transient as functions of test time. Body current, 5.5 mA.

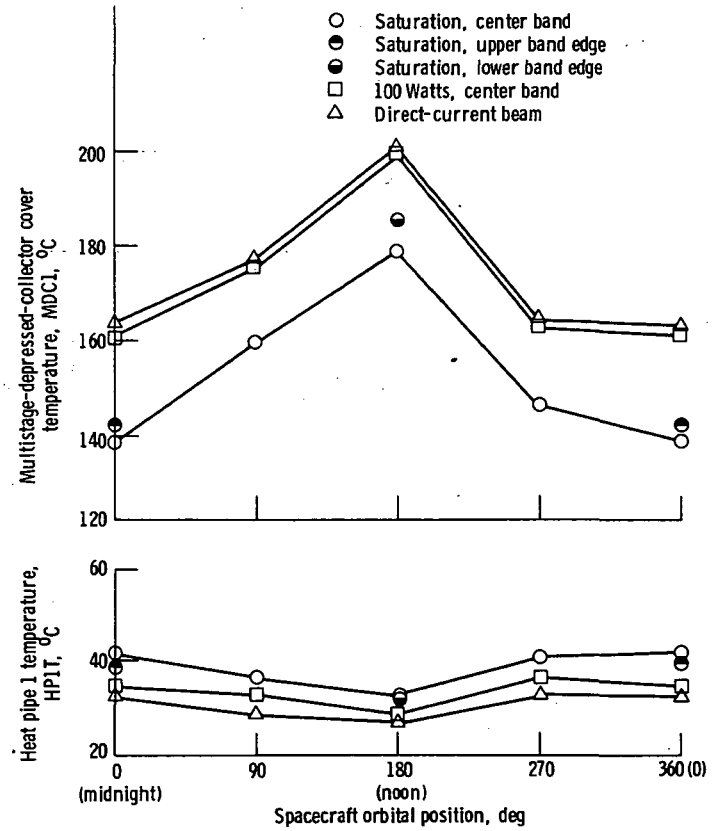

Figure 26. - Multistage-depressed-collector cover and approximate output-stage-tube baseplate temperatures as function of operating conditions and spacecraft orbital position in preeclipse testing period.

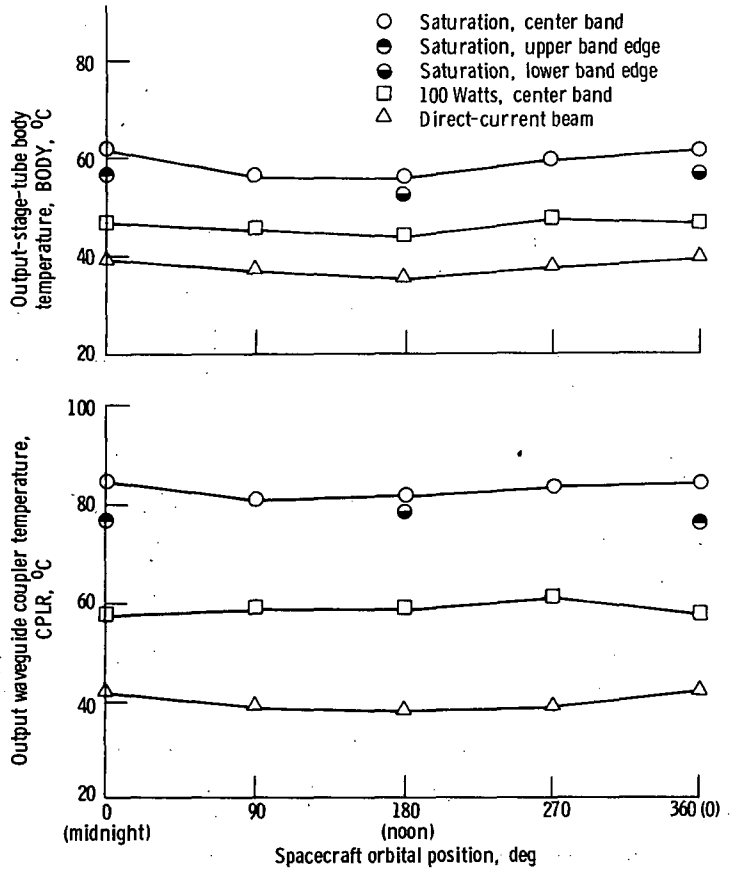

Figure 27. - Output-stage-tube body and output waveguide coupler temperatures as functions of operating conditions and spacecraft orbital position in preeclipse testing period.

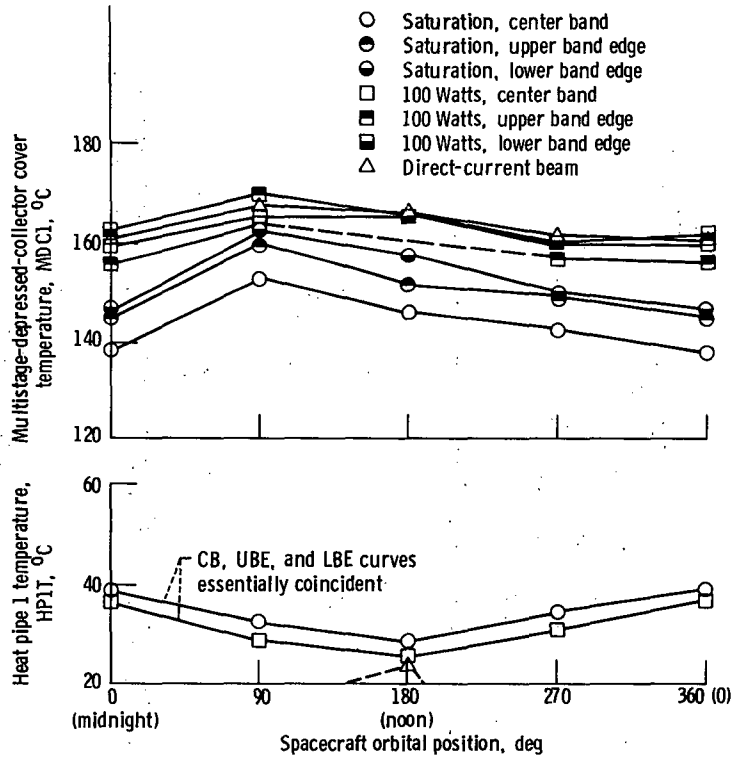

Figure 28. - Multistage-depressed-collector cover and approximate output-stage-tube baseplate temperatures as function of operating conditions and spacecraft orbital position in posteclipse testing period.

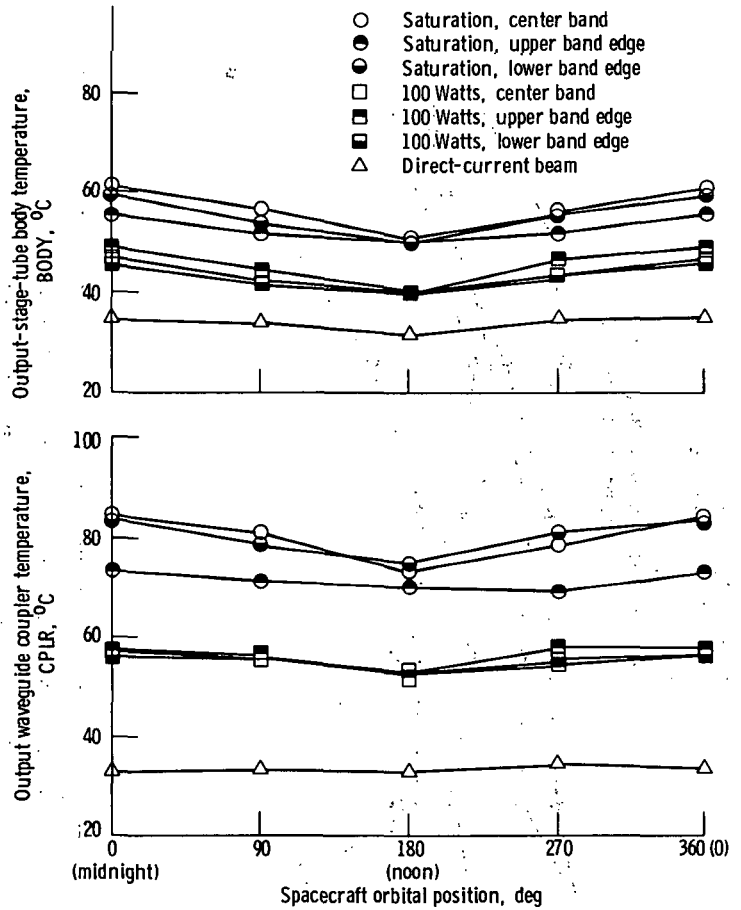

Figure 29. - Output-stage-tube body and output waveguide coupler temperatures as functions of operating conditions and spacecraft orbital position in posteclipse testing period.

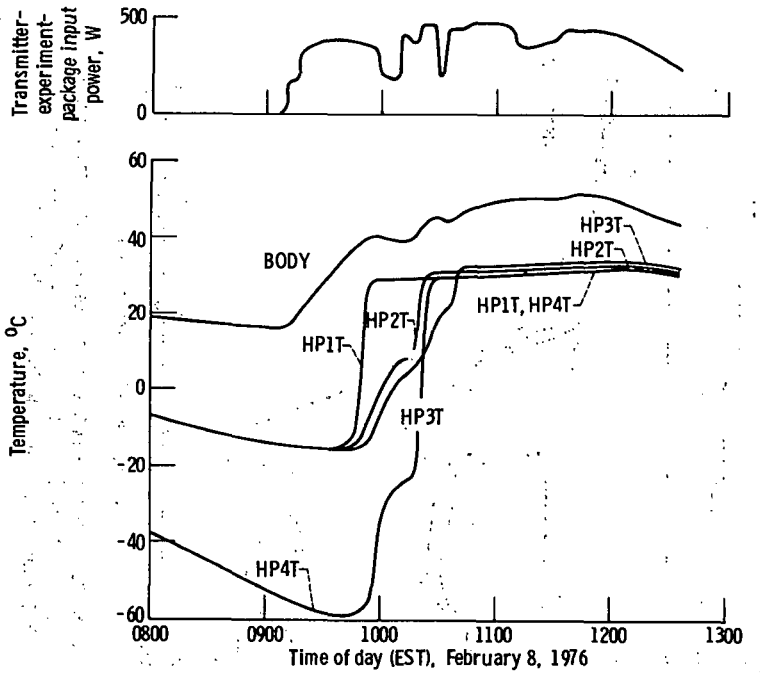

Figure 30. - Output-stage-tube body and selected variable-conductance heat pipe system temperatures and transmitter-experiment-package input power as function of time for initial VCHPS startup sequence after CTS launch.

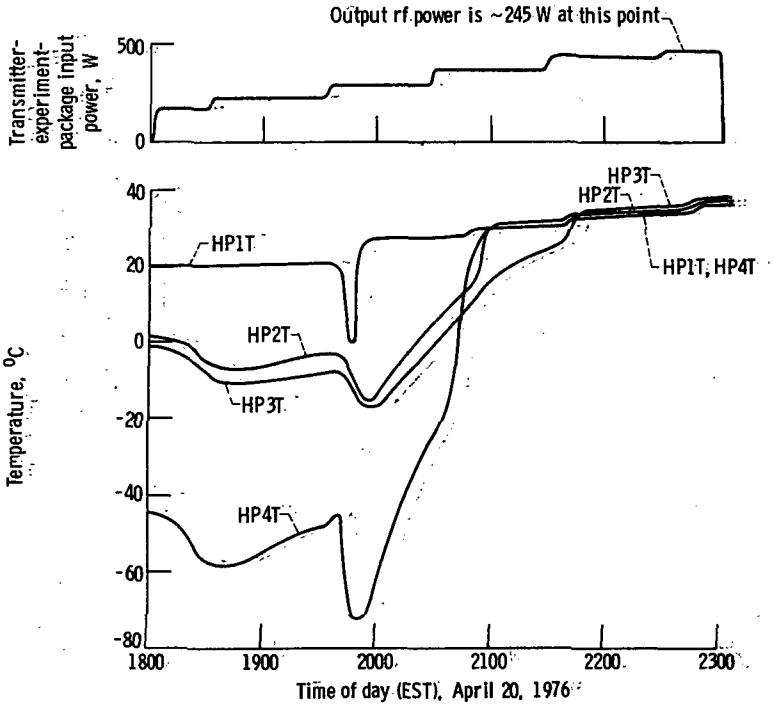

Figure 31. - Selected variable-conductance heat pipe system temperatures and transmitter-experiment-package input power for initial VCHPS turnon sequence following first eclipse period.

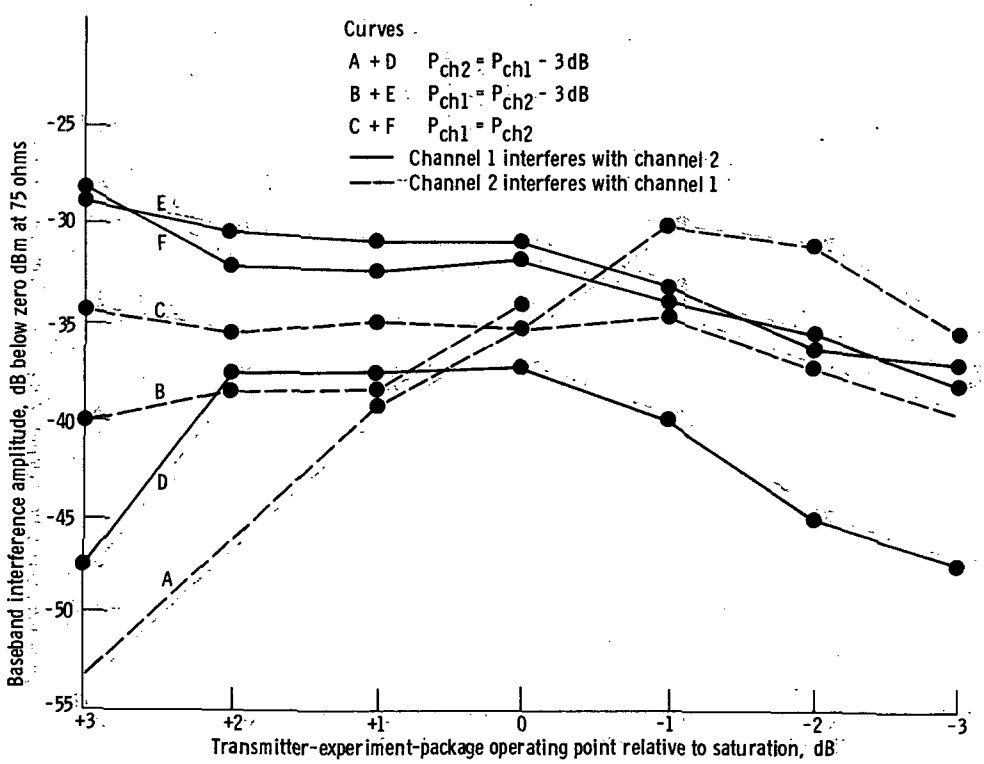

Figure 32. - Dual-channel video crosstalk characteristics.

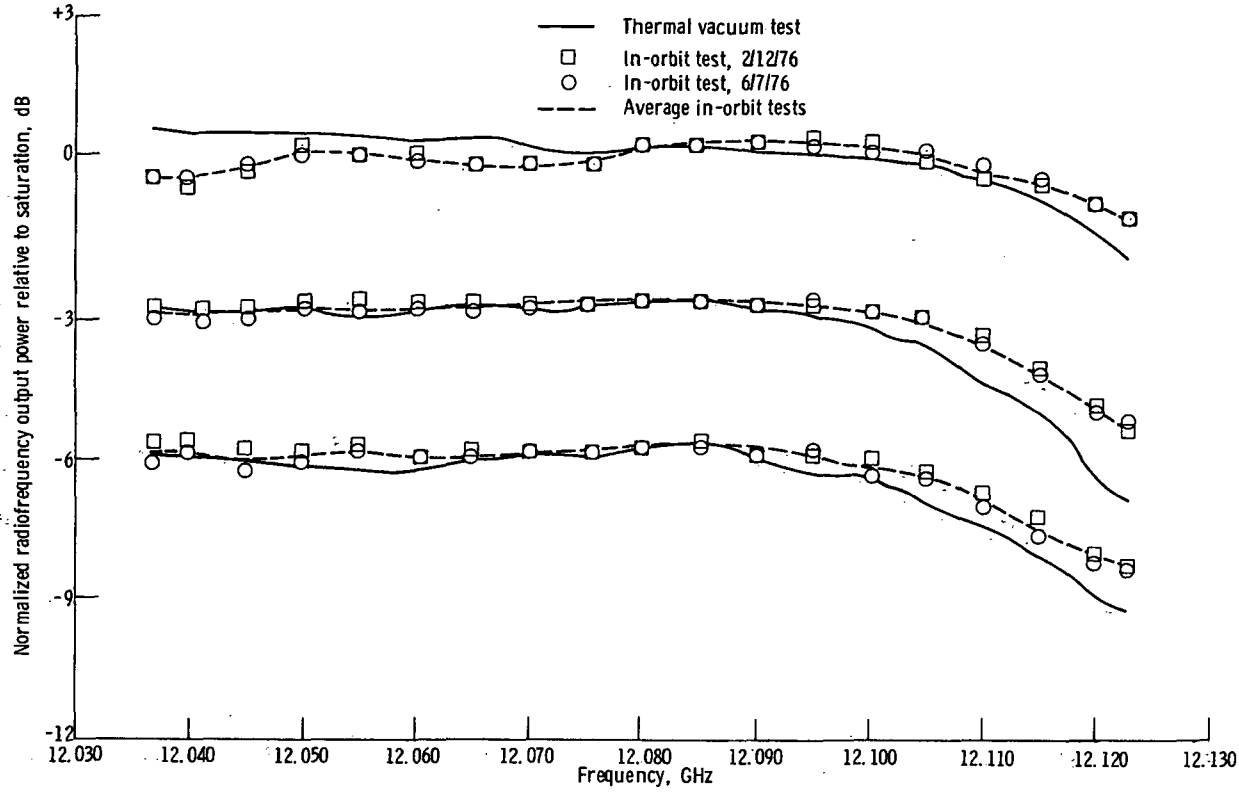

Figure 33. - Output-stage-tube normalized radiofrequency output power as function of frequency.

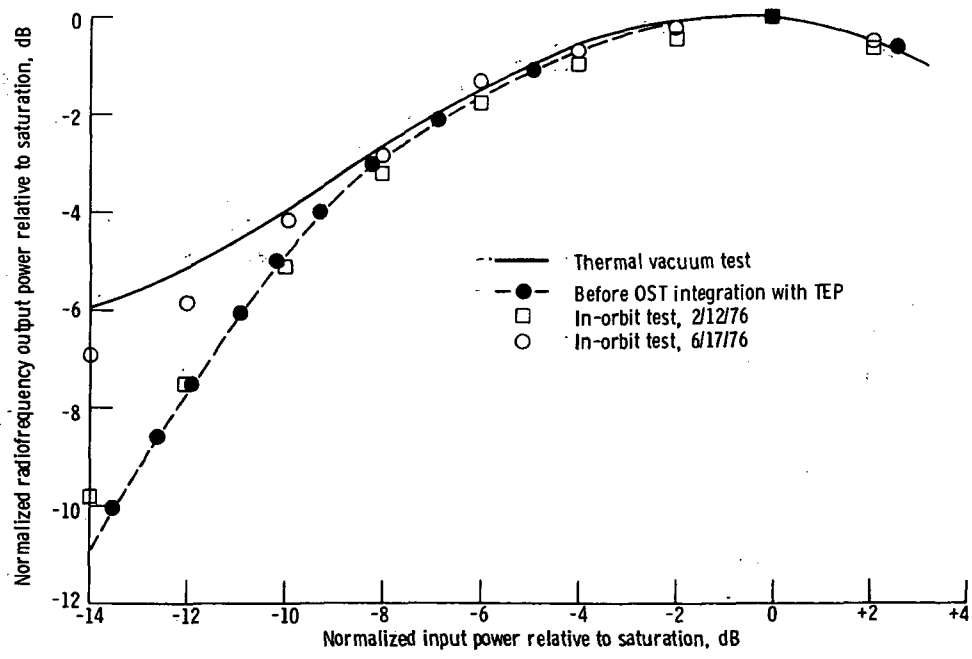

Figure 34. - Output-stage-tube preflight and in-orbit normalized radiofrequency output power as functions of input power - frequency, 12.080 GHz.

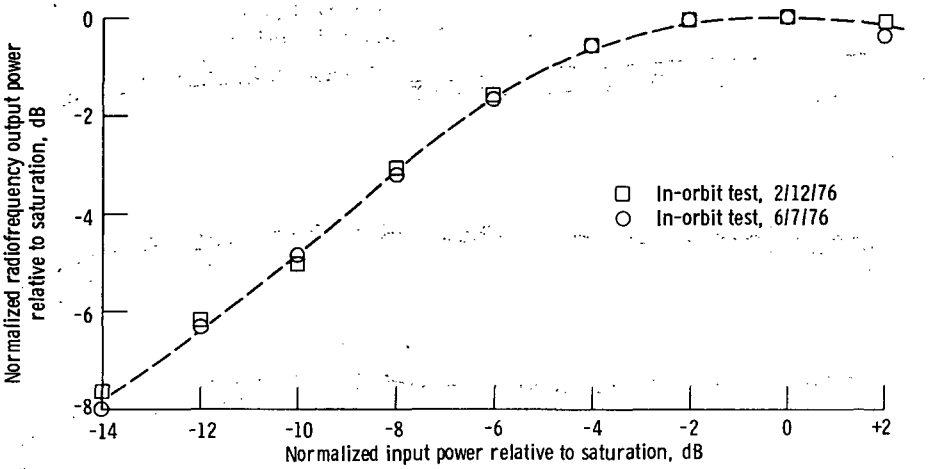

Figure 35. - Output-stage-tube in-orbit normalized radiofrequency output power as function of input power - frequency, 12.038 GHz.

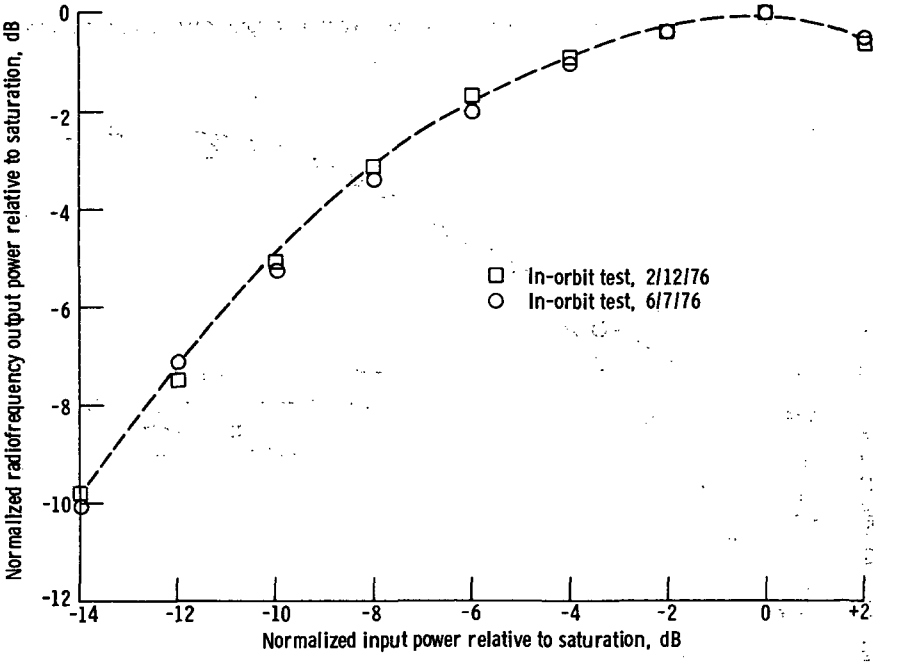

Figure 36. - Output-stage-tube in-orbit normalized radiofrequency output power as function of input power - frequency, 12.080 GHz.

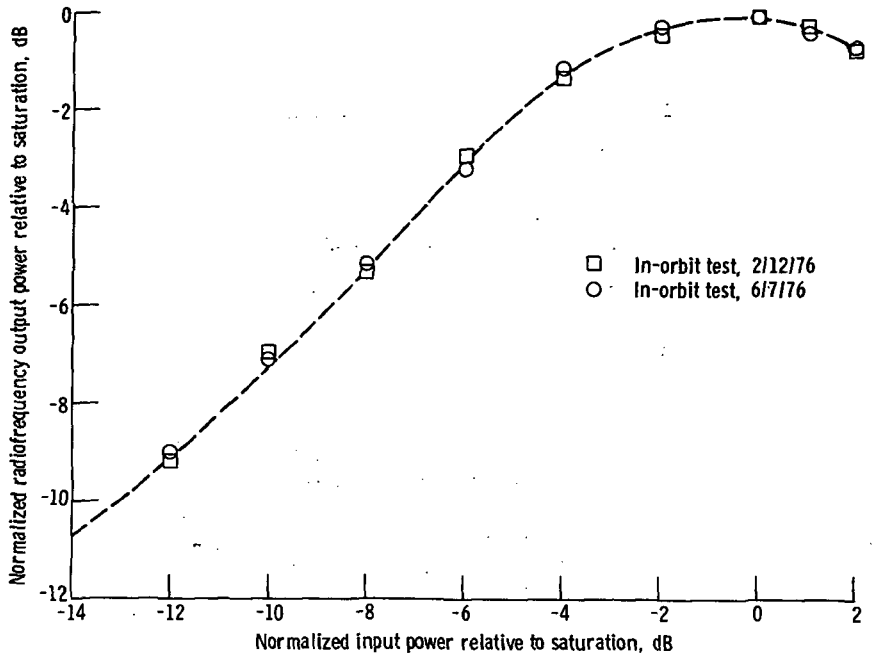

Figure 37. - Output-stage-tube in-orbit normalized radiofrequency output power as function of input power - frequency, 12.123 GHz.

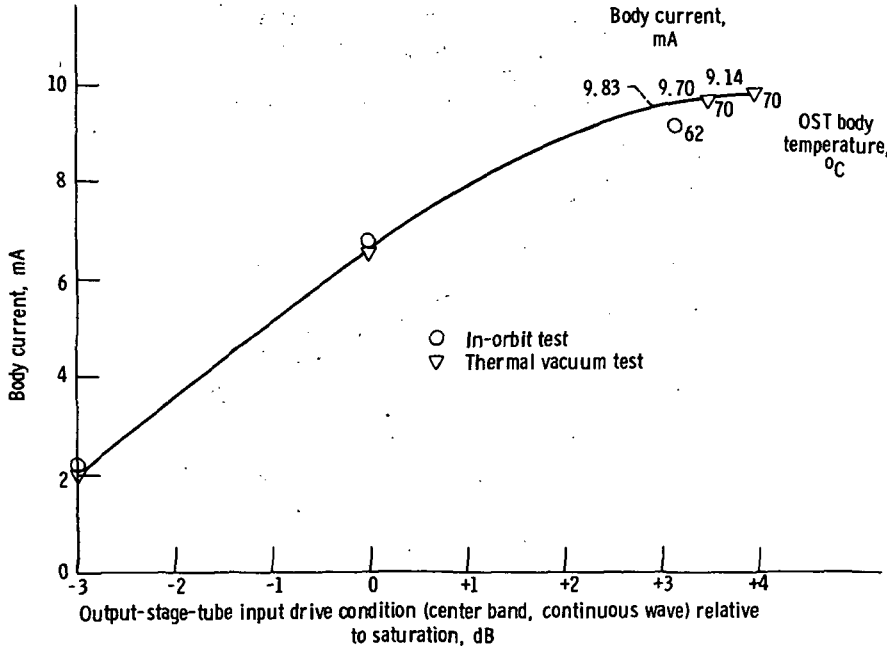

Figure 38. - Output-stage-tube overdrive test results.

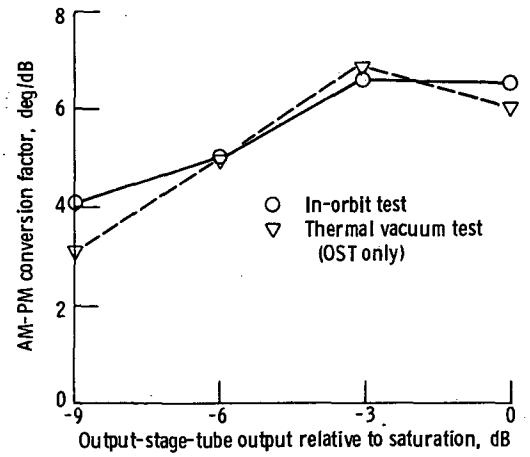

Figure 39. - Output-stage-tube amplitude modulation - phase modulation conversion test results. Downlink band 1 (TB1). (Transponder configuration: receiver 1; FET 1; TWT 2; attenuator 2, 5 dB.)

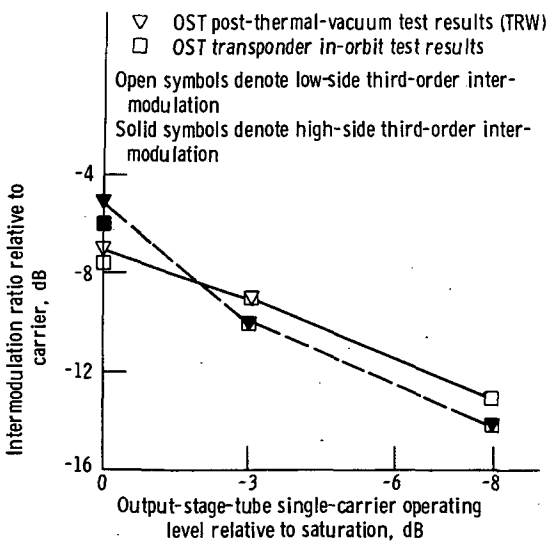

Figure 40. - Output-stage-tube signal-to-intermodulation-ratio test results.

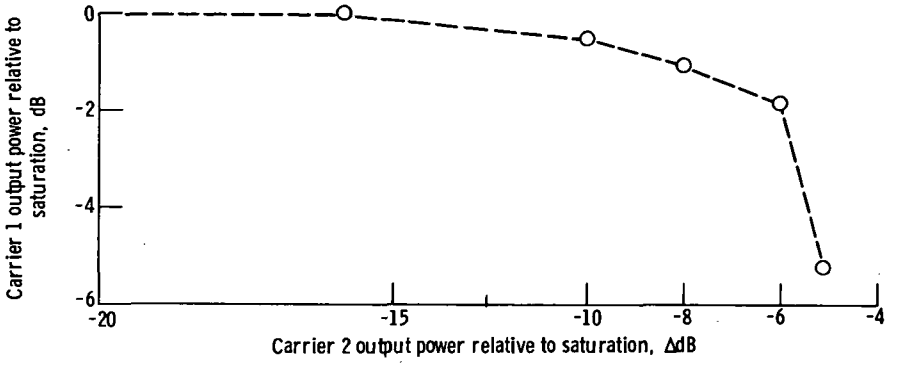

Figure 41. - Output-stage-tube transponder gain suppression test results.

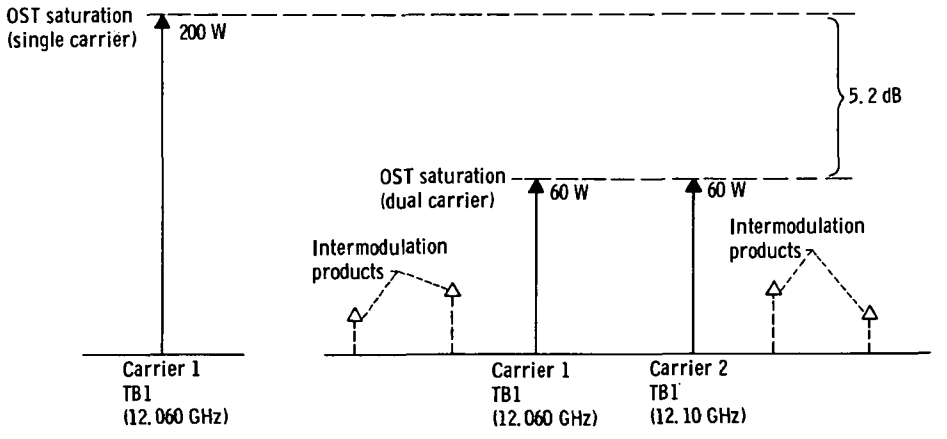

(a) Single-carrier operation.

(b) Dual-carrier operation.

Figure 42. - Output-stage-tube gain suppression characteristics. (For two-equal-carrier operation; each carrier suppressed 5.2 dB referenced to single-carrier operation.)

NATIONAL AERONAUTICS AND SPACE ADMINISTRATION
WASHINGTON, D.C. 20546

OFFICIAL BUSINESS
PENALTY FOR PRIVATE USE $300

THIRD-CLASS BULK RATE

POSTAGE AND FEES PAID
NATIONAL AERONAUTICS AND
SPACE ADMINISTRATION
451

U.S.MAIL

POSTMASTER: If Undeliverable (Section 158 Postal Manual) Do Not Return

"The aeronautical and space activities of the United States shall be conducted so as to contribute . . . to the expansion of human knowledge of phenomena in the atmosphere and space. The Administration shall provide for the widest practicable and appropriate dissemination of information concerning its activities and the results thereof."

—NATIONAL AERONAUTICS AND SPACE ACT OF 1958

NASA SCIENTIFIC AND TECHNICAL PUBLICATIONS

TECHNICAL REPORTS: Scientific and technical information considered important, complete, and a lasting contribution to existing knowledge.

TECHNICAL NOTES: Information less broad in scope but nevertheless of importance as a contribution to existing knowledge.

TECHNICAL MEMORANDUMS: Information receiving limited distribution because of preliminary data, security classification, or other reasons. Also includes conference proceedings with either limited or unlimited distribution.

CONTRACTOR REPORTS: Scientific and technical information generated under a NASA contract or grant and considered an important contribution to existing knowledge.

TECHNICAL TRANSLATIONS: Information published in a foreign language considered to merit NASA distribution in English.

SPECIAL PUBLICATIONS: Information derived from or of value to NASA activities. Publications include final reports of major projects, monographs, data compilations, handbooks, sourcebooks, and special bibliographies.

TECHNOLOGY UTILIZATION PUBLICATIONS: Information on technology used by NASA that may be of particular interest in commercial and other non-aerospace applications. Publications include Tech Briefs, Technology Utilization Reports and Technology Surveys.

Details on the availability of these publications may be obtained from:

SCIENTIFIC AND TECHNICAL INFORMATION OFFICE

NATIONAL AERONAUTICS AND SPACE ADMINISTRATION

Washington, D.C. 20546